

# **SANDIA REPORT**

SAND97-1423 • UC-910

Unlimited Release

Printed June 1997

## **Design Considerations for the Development of a Space Qualification Short Wavelength Imaging Fourier Transform Spectrometer (SWIFTS)**

Russell E. Abbink

Prepared by  
Sandia National Laboratories  
Albuquerque, New Mexico 87185 and Livermore, California 94550

Sandia is a multiprogram laboratory operated by Sandia  
Corporation, a Lockheed Martin Company, for the United States  
Department of Energy under Contract DE-AC04-94AL85000.

Approved for public release; distribution is unlimited.



**Sandia National Laboratories**

Issued by Sandia National Laboratories, operated for the United States Department of Energy by Sandia Corporation.

**NOTICE:** This report was prepared as an account of work sponsored by an agency of the United States Government. Neither the United States Government nor any agency thereof, nor any of their employees, nor any of their contractors, subcontractors, or their employees, makes any warranty, express or implied, or assumes any legal liability or responsibility for the accuracy, completeness, or usefulness of any information, apparatus, product, or process disclosed, or represents that its use would not infringe privately owned rights. Reference herein to any specific commercial product, process, or service by trade name, trademark, manufacturer, or otherwise, does not necessarily constitute or imply its endorsement, recommendation, or favoring by the United States Government, any agency thereof or any of their contractors or subcontractors. The views and opinions expressed herein do not necessarily state or reflect those of the United States Government, any agency thereof or any of their contractors.

Printed in the United States of America. This report has been reproduced directly from the best available copy.

Available to DOE and DOE contractors from  
Office of Scientific and Technical Information  
PO Box 62  
Oak Ridge, TN 37831

Prices available from (615) 576-8401, FTS 626-8401

Available to the public from  
National Technical Information Service  
US Department of Commerce  
5285 Port Royal Rd  
Springfield, VA 22161

NTIS price codes  
Printed copy: A08  
Microfiche copy: A01

SAND 97-1423  
Unlimited Release  
Printed June 1997

Distribution  
Category UC-910

## **DESIGN CONSIDERATIONS FOR THE DEVELOPMENT OF A SPACE QUALIFICATION SHORT WAVELENGTH IMAGING FOURIER TRANSFORM SPECTROMETER (SWIFTS)**

Russell E. Abbink  
Optics & Exploratory Technologies Department  
Sandia National Laboratories  
P.O. Box 5800  
Albuquerque, New Mexico, 87185-0439

### **Abstract**

This document is the final report on work performed at Sandia National Laboratories during FY 1992 and 1993 for a Laboratory Directed Research and Development (LDRD) program to look at problems associated with the design and long term operation of a short wavelength imaging Fourier Transform (FT) spectrometer for use in space. In attempts to answer two fundamental questions: is a FT spectrometer with a resolution of  $1\text{cm}^{-1}$  covering the silicon detector wavelength range of 0.4 to 1.1 microns feasible in a long life space instrument and, if so, is it the best method of obtaining the desired information? Emphasis has been on identifying methods which minimize reliance on precision mechanical alignment and precise velocity control. An important consideration has also been to develop methods which will be compatible with a variety of self-scanning solid state imaging devices. A breadboard instrument was constructed using cube corner retroreflectors and a laser diode position reference. Some preliminary results are reported. This work is primarily intended to act as an aid to engineers at Sandia who wish to pursue the fabrication of a flight qualified instrument. The theoretical parts are intended to be somewhat tutorial in nature to aid the engineer who is not familiar with FT spectroscopy.



## Contents

1.0 Introduction . . . . .	1
2.0 Fourier Transform Spectrometer (FTS) principles of operation . . . . .	2
2.1 Response to mirror movement . . . . .	4
2.2 Sampling interval . . . . .	4
2.3 Total mirror travel required for a given spectral resolution . . . . .	6
2.4 Instantaneous field-of-view . . . . .	7
3.0 Comparison with a grating type spectrometer . . . . .	8
3.1 Multiplex advantage . . . . .	8
3.2 Throughput comparison . . . . .	9
3.3 Response to signal intensity fluctuations . . . . .	11
4.0 Requirements for a practical FTS. . . . .	13
4.1 Mirror alignment stability requirements . . . . .	13
4.2 Eliminating signal fluctuation or its effects . . . . .	16
4.3 Amplitude dynamic range and amplitude resolution . . . . .	20
4.4 Sampling interval accuracy requirements . . . . .	23
4.5 Methods of sample interval generation . . . . .	24
4.6 Aspects unique to an imaging FT spectrometer . . . . .	27
5.0 The SWIFTS breadboard instrument . . . . .	29
5.1 Design goals . . . . .	29
5.2 Components of the primary optical system . . . . .	29
5.3 Moving mirror suspension and drive system . . . . .	33
5.4 Reference laser . . . . .	37
5.5 Electronics and signal processing . . . . .	42
6.0 Results and conclusions . . . . .	45
References . . . . .	47

---

## Figures

2.1 Basic Michelson Interferometer . . . . .	3
4.1 Two Schemes for Reducing Mirror Alignment Sensitivity . . . . .	15
4.2 Interferometer with Offset Retroreflectors . . . . .	19
5.1 Primary Optical Path of the SWIFTS Breadboard . . . . .	30
5.2 View Looking Into Retroreflector Axis of Symmetry. . . . .	32
5.3 Moving Mirror Drive and Suspension System . . . . .	34
5.4 Flexure Spring Designs. . . . .	35
5.5 Optical Path of SWIFTS Laser Diode Interferometer. . . . .	38
5.6 Reference Frequency Doubling Scheme . . . . .	39
5.7 Laser Interferometer with Components Added for Direction Sensing. . . . .	40
5.8 SWIFTS Breadboard Electronics Block Diagram. . . . .	43

## 1.0 Introduction

This document is the final report on work performed at Sandia National Laboratories during FY1992 and 1993 for a Laboratory Directed Research and Development (LDRD) program to look at problems associated with the design and long term operation of a short wavelength imaging Fourier Transform (FT) spectrometer for use in space. It attempts to answer two fundamental questions: is a FT spectrometer of the desired resolution and wavelength range feasible in a long life space instrument and, if so, is it the best method for obtaining the desired information? Emphasis has been on identifying methods which minimize reliance on precision mechanical alignment and precise velocity control, allowing operation at short wavelengths within the solar reflectance region of the spectrum. An important consideration has also been to develop methods which will be compatible with a variety of self-scanning solid state imaging devices. The project has not attempted to look for completely new and novel approaches to interferometry but has attempted to determine the minimum requirements for a space qualified interferometer, starting with the classical Michelson configuration. This work is primarily intended to act as an aid to engineers at Sandia who wish to pursue the fabrication of a flight qualified instrument. The theoretical parts are intended to be somewhat tutorial in nature to aid the engineer who is not familiar with FT spectroscopy.

Motivation for the program has come mainly from the needs of the Earth environmental research community and the nuclear non-proliferation community, for sensitive, rugged spectrometers with high spectral resolution. Within the solar reflectance region of about 0.3 to 3.9 microns a number of important observations can be made. Common atmospheric gasses such as O<sub>3</sub>, O<sub>2</sub>, NO<sub>2</sub>, CO<sub>2</sub>, and water vapor have absorption lines in this region. Observation of sunlight either directly through the atmosphere or by reflection from the earth surface can be used to determine the amount of these gasses in the atmosphere and possibly to profile their concentration as a function of altitude. Observation of clouds at a combination of absorbing and non-absorbing wavelengths can yield information such as cloud type and amount, cloud height, phase, particle size, and thickness. Many surface materials such as vegetation and minerals can also be identified and characterized from solar spectral reflectance signatures.

Multispectral imagers such as the Landsat Thematic Mapper, MODIS, and MTI produce images in only a discrete number of spectral bands, with each band being determined by a fixed wavelength bandpass filter. Thus each instrument is somewhat limited to applications using these specific wavelengths. Recently there has been increased interest in hyperspectral instruments, such as AVIRIS, which can produce simultaneous images at a large number of closely spaced wavelengths. This allows the data analyst to develop optimal retrieval algorithms for originally anticipated phenomena and to use the same instrument, without modification, for new studies not anticipated by the original designers. This is of great importance for an instrument designed for space, where it can not be easily accessed for modification. Various techniques for obtaining the wavelength discrimination

include wedge interference filters, diffraction gratings, prisms, and various forms of interferometers, each offering its own set of advantages and disadvantages. It is our belief that at least in some situations the FT interferometer may have advantages over other forms of hyperspectral imagers, even at short wavelengths where traditionally it has been avoided because of stringent mechanical requirements.

The main body of this report is divided into four parts. The first part describes the classical Michelson interferometer and derives the basic equations of operation necessary for evaluating the tolerances required to make a real instrument work. In the second part the interferometer based instrument is compared with its chief competitor, the grating based instrument. In the third part a number of issues are discussed which must be addressed in designing a practical instrument. As a part of this project a breadboard interferometer was built to allow some of the concepts to be evaluated. The fourth part of the report describes this breadboard.

It was our intention to be able to use the breadboard instrument to make a number of measurements through the earth atmosphere in order to compare the performance of several different operating modes. The breadboard was assembled and some preliminary testing was done but funding cutoff and loss of key project personnel precluded any further development. It is our hope that this report and the interferometer breadboard will prove useful to those wishing to pursue this work further.

## **2.0 Fourier Transform Spectrometer (FTS) principles of operation**

The principles of Fourier transform spectroscopy have been widely discussed in the literature, however, a brief review is appropriate here. A basic Michelson interferometer for use in collimated light is shown in Figure 2.1. It consists of a beam splitter, a phase compensator, a fixed mirror, a moving mirror, a mirror position indicator, a focusing lens, and a detector. The instrument is aligned so that the two mirrors are optically parallel. The incoming light is split into two paths by the beam splitter. Light reflected by the beam splitter is again reflected by the fixed mirror and then transmitted through the beam splitter and lens to the detector. Light originally transmitted by the beam splitter is reflected from the moving mirror back to the beam splitter where it is reflected through the lens onto the detector. The phase compensator is simply a piece of glass of the same type and thickness as the glass on which the beam splitter coating is deposited. Its function is to provide equal dispersion (i.e. equal optical path distance at all wavelengths) for both legs of the interferometer. The resulting detector output is then the vector sum of the signals from these two paths. Signal amplitude is recorded as a function of mirror position as the mirror is moved over a specific range of travel. This record is commonly referred to as an interferogram. The interferogram can then be Fourier transformed to recover the input spectrum of the light. Spectral resolution is determined by the length of travel of the mirror over which data is recorded and the required minimum sampling rate is determined by the shortest wavelength and spectral bandwidth being observed.

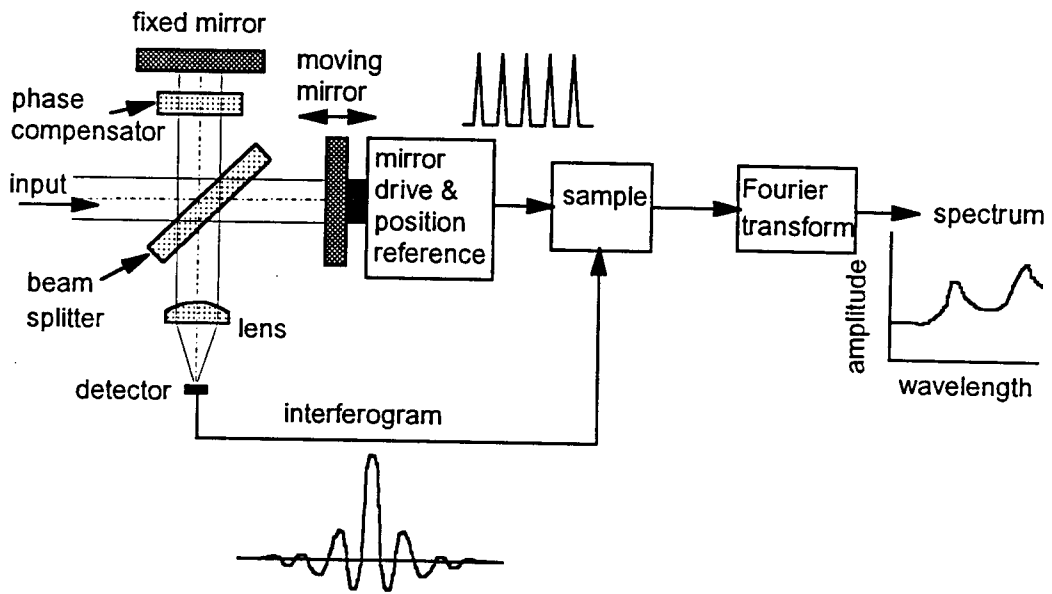


Figure 2.1 Basic Michelson Interferometer

## 2.1 Response to mirror movement

Let us look first at the instrument response to a monochromatic input of wavelength,  $\lambda$ , and intensity,  $\Phi$ . At the point in the mirror travel where the optical path distance to the detector is identical for the two paths the two components will be in phase and add constructively. For an ideal 50/50 beam splitter the detected intensity would then be  $\Phi/2$  since half the signal energy is lost by the beam splitter. If we now move the mirror a distance of  $\lambda/4$  in either direction the relative phase of the two paths will change by  $\lambda/2$  since the light travels twice the distance the mirror is moved. At this point the detected intensity will be zero. As the mirror is moved the detector output will be cosinusoidal as a function of mirror position with a peak-to-peak intensity of  $\Phi/2$  and a period equal to a mirror travel distance of  $1/2$  wavelength. If we let,  $x$ , designate the mirror travel distance from the center position then we can express the response as,

$$I = K(1 + \cos(4\pi x/\lambda)), \quad (2.1)$$

where  $I$  is the detector response and  $K$  is a constant depending on the input intensity, optical system losses and detector responsivity. If several monochromatic signals of different wavelengths are present in the input the output will be the sum of the sinusoidal components produced by each wavelength. This can be extended to any band limited spectrum of input wavelengths based on the fact that any band limited signal can be broken up into its Fourier components. Note that at the point in the mirror travel where both paths are equal, ( $x = 0$ ), the signals from the two branches are in phase regardless of wavelength. As we move away from this center position in either direction the sinusoid produced by one wavelength will, in general, be out of phase with the sinusoids produced by other wavelengths. Thus, we would expect the interferogram to have a large peak at the equal path length or center position, where all components add constructively, and to have diminished amplitude everywhere else. We should note also that the interferogram will be symmetrical about this center position, with the waveform on one side of center being a mirror image of that on the other side. Since both sides contain identical information we could rightly reason that, in this ideal case, data need be recorded only on one side. In any real interferometer there is usually some amount of uncompensated dispersion. Thus, the equal path distance mirror position will be slightly different for each wavelength, resulting in an interferogram which is not perfectly symmetrical about any one point. Because of this it is common practice to record at least a part of the second side of the interferogram, allowing the phase dispersion to be determined mathematically.

## 2.2 Sampling interval

In digitizing the output of the spectrometer it is desirable to represent the signal with as few data points as necessary. According to the Nyquist sampling theorem a signal limited by a low pass filter can be exactly reconstructed if it is sampled at intervals of less than  $\lambda/2$  for the shortest wavelength present in the signal. Thus, in order to recover all information from the interferogram it is not necessary to continuously record the waveform but only to sample it periodically. If the shortest wavelength represented in the interferogram is  $\lambda_s$ , then we need to sample the signal at mirror position intervals,  $dx$ , not exceeding,

$$dx = \lambda_s/4. \quad (2.2)$$

However, since any realizable instrument will be spectrally limited at both the long and short wavelength ends it is possible in some cases to further increase the sampling interval. Let  $\sigma = 1/\lambda$ . ( $\sigma$  is referred to as the wave number, with units of  $\text{cm}^{-1}$ ). Then let  $\sigma_u$  and  $\sigma_L$  be the upper and lower wavenumbers respectively in a band limited signal, with the requirement that they be selected such that,

$$\sigma_u = k(\sigma_u - \sigma_L), \quad (2.3)$$

where  $k$  is any positive non zero integer. Then it can be shown (Wolf 1967, pp. 274-279) that we can increase the sampling interval to,

$$dx = 1/(4(\sigma_u - \sigma_L)) \quad (2.4)$$

Combining equations 2.4 and 2.3 this can also be written,

$$dx = k/(4\sigma_u). \quad (2.5)$$

Sampling interval here is again expressed as a function of mirror position.

As an example let us look at the sampling interval required to record the output of a spectrometer limited in bandwidth by the response of a silicon detector. We will assume for our purposes that the wavelength range is limited to 0.4 to 1.1 microns. ( $25,000$  to  $9,090.9 \text{ cm}^{-1}$ ). From equation 2.2 we see that the required maximum sampling interval is  $0.4/4 = 0.1$  microns. However, since the signal is band limited on both the upper and lower ends we can use equation 2.4 to test for a relaxation of this sampling distance. Solving for  $k$  we get,

$$k = \sigma_u/(\sigma_u - \sigma_L) = 25,000/(25,000 - 9,090.9) = 1.57$$

Since  $k$  must be an integer we can choose a value of 1 or 2. If we choose a value of 1, then equation 2.5 shows that there is no improvement in the sampling interval requirement. If we choose a value of 2 then there will be a factor of two improvement, allowing samples to be taken at 0.2 micron intervals, provided that  $\sigma_2$  remains at  $25,000 \text{ cm}^{-1}$ . This cannot be done, however, without adjusting the value of  $\sigma_1$  to satisfy equation 2.3. Solving equation 2.3 for  $\sigma_L$  given  $k = 2$  and  $\sigma_u = 25,000$  we get  $\sigma_L = 12,500 \text{ cm}^{-1}$ . Thus to cover the entire silicon detector spectrum without the use of additional bandpass filters we will require a sampling interval of 0.1 microns.

The values of  $\sigma_u$  and  $\sigma_L$  used in calculations must be selected carefully, keeping in mind that a real band pass filter or detector does not have infinite slope or infinite out-of-band rejection.

### 2.3 Total mirror travel required for a given spectral resolution

Consider two monochromatic sources at wave numbers  $\sigma_1$  and  $\sigma_2$  with separation  $\Delta\sigma = \sigma_2 - \sigma_1$ . Then let  $x = L$  be the mirror travel from the center position required to produce a  $2\pi$  phase shift between the signals at the two frequencies. Stated in another way  $L$  is the distance the mirror must travel from center in order to observe one full cycle of the difference wave number. From equation 2.1 we see that this occurs when,

$$4\pi L\sigma_2 = 4\pi L\sigma_1 + 2\pi. \quad (2.6)$$

Solving for  $L$  we get,

$$L = 1/(2\Delta\sigma) \quad (2.7)$$

For an unapodized interferometer, that is, one for which the gain is not a function of mirror position, equation 2.7 is considered to be the relationship between resolution and mirror travel. For the complete two-sided interferogram the mirror must travel this distance on both sides of center.

This result may also be obtained in another, perhaps, more enlightening way. A monochromatic source at wavenumber  $\sigma_0$  is an impulse function in the wavenumber domain. If we take the Fourier transform of this impulse we get an infinite series of cosine functions in the spatial domain (mirror position). A finite travel of the mirror over  $\pm L$  is equivalent to truncating the series at these limits. Taking the inverse transform of this truncated series produces a sinc function in the wavenumber domain with the first zeros at  $\sigma = \sigma_0 \pm 1/(2L)$ , yielding a result equivalent to equation 2.7. Because the result of truncating the mirror travel is to create oscillations in the form of the sinc function in the inverse transformed spectrum it has become common practice to apodize the interferogram before the inverse transform is performed. For example, the interferogram might be multiplied by a triangle apodization function with the value of 1 at  $x = 0$  and 0 at  $x = L$ . The effect is to reduce the oscillations but to widen or spread the energy of the spectral line over a larger range. A variety of apodization functions is discussed in the literature (Wolf 1967, p. 284).

Combining equations 2.7 and 2.4 we see that the total number of samples,  $N$ , required for a two sided interferogram is,

$$N = 2L/dx = 4(\sigma_u - \sigma_L)/\Delta\sigma, \quad \sigma_u = k(\sigma_u - \sigma_L), \quad k = 1, 2, 3, \dots \quad (2.8)$$

Again referring to the example of section 2.2 the number of samples required to record a double sided interferogram of the 0.4 to 1.1 micron spectrum with a resolution of  $1 \text{ cm}^{-1}$  will be,

$$N = 4 * 25,000 / 1.0 = 100,000$$

If we wish to obtain the spectrum from the interferogram we might want to constrain this number to a power of 2 in order to more efficiently use a Fast Fourier Transform (FFT) algorithm. Thus, we want to take a minimum of  $2^{17} = 131,072$  samples, either by increasing  $L$  or decreasing  $dx$ . We could also consider interpolation of the required 100,000 data samples.

#### 2.4 Instantaneous field-of-view

We define instantaneous field-of-view as the largest source solid angle,  $\Omega$ , which can be viewed without severely degrading the peak-to-peak amplitude of the interferogram. Consider two monochromatic rays going through the interferometer, one on axis and the other at an angle,  $\alpha$ , to the axis. As the mirror moves these two rays will produce sinusoidal responses at the detector which are out of phase with each other. At a phase difference of 180 degrees the signals will cancel each other, so, we might consider the angle producing this phase shift as the maximum acceptance angle. For the maximum mirror displacement,  $L$ , the path length difference between these two rays is,

$$\Delta x = 2(L - L \cos \alpha)$$

Using the small angle approximation for  $\cos \alpha$ , we get,

$$\Delta x = L \alpha^2$$

Substituting for  $L$  from equation 2.7 we can write,

$$\Delta x = \alpha^2 / (2\Delta\sigma) \tag{2.9}$$

For the condition where the two signals are 180 degrees out of phase we have,

$$\Delta x = \lambda/2 = 1/(2\sigma).$$

Combining this with equation 2.9 and rearranging we get,

$$\alpha^2 = \Delta\sigma/\sigma$$

and finally,

$$\Omega = \pi \alpha^2 = \pi \Delta\sigma/\sigma. \tag{2.10}$$

Thus, the usable solid angle is a function only of the resolution and wave number. The worst case, that is, the one leading to the smallest usable solid angle occurs at the highest wave number. It can be shown by integrating the response function over all values of  $\alpha$  that for the criterion chosen, i.e. a 180 degree phase change between axial and extreme rays, the detected sinusoid amplitude at the mirror position,  $L$ , will be 0.64 that at the center. The amplitude does not go to zero until  $\alpha$  is twice this value. Since the detector

area would have to be increased to accept a larger value of  $\alpha$ , equation 2.10 is usually considered the practical limit.

A numerical example will bring out an interesting fact. Let  $\Delta\sigma = 1 \text{ cm}^{-1}$  and  $\sigma = 25,000 \text{ cm}^{-1}$ . Then  $\Omega = 1.26 \times 10^{-4} \text{ sr}$  and  $2\alpha = 0.72 \text{ degrees}$ . This last quantity is of interest because it shows that in an imaging system the angular subtense of a single pixel would have to be 0.72 degrees in the image plane to take full advantage of the instantaneous field of view available to the interferometer, even at this very large wave number. This could place severe demands on the optics of even a moderate resolution imaging system. This will take on significance when comparing the interferometer with a grating instrument in the next section.

### 3.0 Comparison with a grating type spectrometer

Given the appropriate conditions the FT spectrometer is capable of providing superior signal to noise ratio compared to a grating instrument of equal collection aperture. Classically, two advantages have been claimed for the FT instrument. The first of these is the multiplex, or Fellgett, advantage and the second is the throughput, or Jacquinot, advantage. A third comparison we will make is in the response to source intensity fluctuations during the measurement period. There are many other comparisons which could be made between FT interferometer based instruments and other ways of making the same measurement but we will limit ourselves in this report to these three.

#### 3.1 Multiplex advantage

The multiplex advantage compares the FT spectrometer with a single slit grating instrument. If there are  $N$  spectral elements to be examined in a time  $T$  the single slit instrument must examine each element in a time  $T/N$  whereas the FT instrument has the entire time,  $T$ , since all spectral elements are viewed simultaneously. (Actually both instruments must make  $N$  measurements in the time,  $T$ , giving them both the same detector electrical bandwidth requirement, but, the interferometer samples the same signal  $N$  times.) Thus, we would expect an improvement of  $N^{1/2}$  in the signal to random noise ratio of the interferometer if all else were equal. This would indeed be the case if the FT system were internal noise dominated, i.e. noise independent of the signal. However, if we are looking at weak absorption spectra in a background continuum the total D.C. signal on the FT detector will be on the order of  $N$  times what it would be on a single element of the grating instrument. Thus, the performance of the FT detector is more likely to be dominated by the background photon flux shot noise. In this case the noise will increase in proportion to  $N^{1/2}$ , completely cancelling the multiplex advantage.

Another fact to consider is that many modern grating based instruments use an  $N$  element photodiode array rather than a single slit reimaged on a single detector element, allowing each element to integrate the signal for the entire time,  $T$ . In defense of the FT instrument, though, we should note that in the example of section 2.4 a value of  $\sigma/\Delta\sigma$  of 25,000 was used, requiring a total of 50,000 data points. These are easily obtained in the FT instrument by moving the mirror. If the grating instrument is to overcome the

multiplex advantage it would require an array of 50,000 separate detector elements (32,000 if only the Si detector range of 9,000 to 25,000  $\text{cm}^{-1}$  is considered.) This is impractically large. Thus, in a practical sense, the FT instrument would retain at least part of its multiplex advantage when measuring large wave number ranges.

In concluding this section we can say that in situations where a relatively small number of spectral elements is of interest, allowing one detector element per spectral element, or where the FT instrument is shot noise limited by a high background continuum, the advantage is in favor of the grating instrument.

### 3.2 Throughput comparison

Throughput comparison usually comes out vastly in favor of the FT instrument. Throughput, or etendue, is defined as the product of instrument entrance pupil area,  $A$ , and the instantaneous solid angle field of view,  $\Omega$ .  $\Omega$ , for the FT spectrometer, was derived in section 2.4. Here we will derive the same quantity for a grating instrument for the purposes of comparison. Consider a grating instrument with entrance pupil area,  $A$ , an effective focal length,  $f$ , to the slit image and a slit with height and width dimensions,  $v$  and  $w$ , respectively, where  $w$  is the dimension in the spectrally dispersive direction. The throughput,  $E_g$ , will then be,

$$E_g = A\Omega_g = A (v/f)(w/f) = A \theta_v \theta_w \quad (3.1)$$

The two quantities in parenthesis are the angular subtenses of the slit. The full  $N$  element spectrum will then cover an angular subtense of,

$$\theta = N \theta_w \quad (3.2)$$

In order to calculate the angular subtense of  $w$  we must choose an appropriate value for  $\theta$ . Although it would be difficult to design an optical system to cover a total angle of 90 degrees it might be appropriate to set this as a working limit. Thus, we set  $\theta = \pi/2$  and substitute this value in equation 3.2 to obtain,

$$\theta_w = \pi/(2N) \quad (3.3)$$

If we let  $k = v/w$  we can express the throughput in the following form:

$$E_g = A k (\theta_w)^2 = A k \pi^2/(4N^2). \quad (3.4)$$

For comparison of this result with equation 2.10 for the FT system let us make the simplifying assumption that the same wave number range is being measured with a maximum wave number denoted by  $\sigma$  at a resolution of  $\Delta\sigma$ . The Nyquist sampling theorem again says that if samples are taken at intervals of  $\sigma/N$  then the resolution will be  $\Delta\sigma = 2\sigma/N$ . Solving for  $N$  and substituting the result in equation 3.4 we get,

$$E_g = A \Omega_g = A (k/16) (\pi \Delta\sigma/\sigma)^2. \quad (3.5)$$

If we assume equal aperture areas for the two types of instruments we can compare this result with equation 2.10 to obtain the ratio,

$$E_g/E_{\text{ft}} = \Omega_g/\Omega_{\text{ft}} = \pi(k/16) \Delta\sigma/\sigma \quad (3.6)$$

From this equation we can see that the grating instrument will fare the best against the FT instrument at poorer spectral resolution and smaller wave number.

A numerical example will again prove enlightening. First we must decide on an appropriate value for  $k$ , the ratio of slit length to width. Multi-element linear arrays are built for grating spectrometer use which have ratios as high as 100. Using this value and the same values for  $\Delta\sigma$  and  $\sigma$  as in the example of section 2.4, we get  $E_g/E_{\text{ft}} = 7.85 \times 10^{-4}$ . Thus, we see that in spite of using a very large optical system field of view and a very large slit ratio the throughput of the grating instrument is much smaller than that of the FT instrument. This is the primary driver for our interest in a short wavelength FT instrument.

Since our interest in this study is not just in spectrometers in general, but especially in imaging spectrometers, it is interesting to compare the two techniques after we add the constraint that the system must form an image. Here we have two spatial dimensions and one spectral dimension to deal with. In the above example we assumed a slit ratio of 100. If we consider using the grating instrument in an imaging system we would probably be constrained to using a square pixel giving a slit ratio of 1. This, of course, makes the throughput 100 times worse. On the other hand, as pointed out in section 2.4, it is doubtful that the full throughput advantage could be realized in the FT instrument, either, in an imaging application. The allowable instantaneous field of view would probably not be controlled by the instrument function but by the required angular image resolution.

As an example let us assume that we wish to form a 256 x 256 pixel image with the FT instrument. Because of the relatively long optical paths in a Michelson interferometer it is difficult to pass large fields of view. For this example we will assume a total field of view of 5 degrees. Thus each pixel will have an angular subtense of  $5 \text{ deg.} / 256 = 0.02 \text{ deg.}$ , giving the instrument a value of  $\Omega_{\text{ft}} = 3.7 \times 10^{-7} \text{ sr}$ . Let us further assume that no modification of the grating instrument field of view, other than setting  $k = 1$ , is necessary to meet this imaging requirement. We can then calculate the grating instrument solid angle from equation 2.15, obtaining a value of  $\Omega_g = 9.9 \times 10^{-10} \text{ sr}$ . Taking the ratio as in equation 2.16 we get,

$$E_g/E_{\text{ft}} = \Omega_g/\Omega_{\text{ft}} = 2.7 \times 10^{-3}$$

Thus, even in a moderate to high resolution imaging system the FT instrument throughput is very large compared to the grating instrument.

A further advantage of the FT instrument is that an  $N \times N$  dimensional array can be used to form the image and extract the spectral information in a time  $T$ , whereas the same array used in a grating based instrument can give only two of the three dimensions. The designer might choose to use one dimension of the array to extract the spectral information and the other dimension to extract a single line of the image. Thus, to form a complete  $N \times N$  image the time available to measure one line of the image is  $T/N$ . For imaging systems the multiplex advantage of the FT instrument remains. In this case it is a multiplexing of spatial and spectral information on the same pixels.

### 3.3 Response to signal intensity fluctuations

Let us consider the effect of overall signal intensity fluctuation as a function of time. This could occur for a number of different reasons. In stellar interferometry fluctuation is common, due to cells of different refractive index moving through the atmosphere across the aperture. It could also be caused by jitter in the telescope line of sight. This could be especially troublesome when viewing a highly structured scene with an imaging spectrometer.

In the grating instrument each spectral element is measured independently of all the others, so, the variance in the measured intensity of a spectral component simply equals the variance in the source intensity at the input aperture. For the FT interferometer the situation is more complex. Consider an input,  $I_{sig}$ , made up of  $N$  spectral components. From equation 2.1 we can write the total intensity function,  $I_s$ , as,

$$I_{sig}(x) = \sum^N A_n (1 + \cos(4\pi x \sigma_n)) = A + \sum^N A_n \cos(4\pi x \sigma_n). \quad (3.7)$$

The average value,  $A$ , or D.C. component is just the sum of the  $A_n$  values. For a continuum covering a large wave number range this could be very large compared to the value of a single component. We can also define a band limited modulating function,  $I_{Mod}$ , for the intensity fluctuation as,

$$I_{Mod}(t) = 1 + \sum^M B_m \cos(\omega_m t + \phi_m) \quad (3.8)$$

which simply describes a time series of  $M$  components of arbitrary frequency, amplitude and phase with an average value of 1.0. For a constant mirror velocity we can express frequency and time in equation 3.7 in terms of an equivalent wave number and mirror position, such that,  $\omega_m t = 4\pi x v_m$ , where  $x = t \cdot \text{velocity}$ , and the  $v_m$  are the set of equivalent wave numbers of the modulating function. Thus, we can write,

$$I_{Mod}(x) = 1 + \sum^M B_m \cos(4\pi x v_m + \phi_m) \quad (3.9)$$

The total signal recorded is then,

$$I_{tot}(x) = I_{sig}(x) \cdot I_{Mod}(x) \quad (3.10)$$

$$\begin{aligned}
&= A + \sum^N A_n \text{Cos}(4\pi x \sigma_n) + A \sum^M B_m \text{Cos}(4\pi x \nu_m + \phi_m) \\
&\quad + (\sum^N A_n \text{Cos}(4\pi x \sigma_n)) (\sum^M B_m \text{Cos}(4\pi x \nu_m + \phi_m)) \quad (3.11)
\end{aligned}$$

The first and second terms are simply the undisturbed average value and components of the original spectrum. The third term is a new spectrum consisting of the frequency components in the modulating spectrum. Notice that the amplitude of this spectrum is multiplied by A, which as we pointed out previously, can be very large compared to the individual  $A_n$ . The fourth term is a product which, when expanded, results in a series of new spectral components with wave numbers equal to the sums and differences, e.g.  $(\sigma_n + \nu_m)$  and  $(\sigma_n - \nu_m)$ , and with amplitudes of  $(1/2) A_n B_m$ .

Clearly the effect of source intensity fluctuation is a much more complex problem for the FT spectrometer than for the grating spectrometer. As a simple example let us look at a spectrum consisting of 10,000 spectral components of approximately equal intensity. If we normalize A to 1.0 then the typical  $A_n$  will be on the order of  $10^{-4}$ . Let us further assume a reasonably stable light source with an overall short term peak-to-peak intensity fluctuation of 0.2%. For simplicity we will assume that this fluctuation consists of a single frequency sinusoid of wave number,  $\nu$ , such that  $\nu$  is within the range of wave numbers constituting the original source spectrum. The amplitude, B, will then be  $10^{-3}$ , ten times greater than one of the component amplitudes of the real spectrum. From the third term in equation 3.11 we see that this will produce a component in the transformed output which is indistinguishable from the real spectral components but with an intensity 10 times greater. The fourth term in equation 3.11 will generate a series of 20,000 components at sum and difference frequencies but with amplitudes on the order of  $0.5 \times 10^{-7}$ . Thus, if one of the sum or difference frequencies is the same as the frequency of a real optical spectral component it will add to or subtract from its apparent amplitude, producing an average error on the order of 0.05%. Depending on the value of  $\nu$  there may be a range of  $\sigma$  values for which one sum and one difference component could both have the same frequency as a real spectral component. In this case the average measurement error could be 0.1% with a peak-to-peak value of 0.2%. This is the same average error we would get with the grating instrument. We use the word, average, here because any particular spectral component, such as a strong absorption line in a continuum could have an actual value much smaller than the average and yet the amount of error signal could be 0.1% of the average, or even greater, making its effect, as a percentage of the true signal amplitude much larger. In general, with a more complex modulation function, the fourth term will have the effect of producing a pseudo-random noise floor with the rms value of the noise being equal to the rms value of the modulating function. This might be considered to be more detrimental to overall measurement accuracy than is the proportional effect in the grating instrument in spite of the fact that the average value of the noise is the same in both cases.

Thus, we have seen that amplitude modulation of the light being measured can have a very profound effect on the accuracy of FT spectrometer measurements compared to grating instruments. The third term in equation 3.11 is particularly bothersome because of the large amplitude of the components produced. It arises not only from external causes such

as the atmosphere or source instability but also from internal components such as the mirror drive mechanism. In a practical instrument measures should be taken to reduce or eliminate this term. In some cases it can be eliminated by simply driving the moving mirror faster or slower to shift the values of  $\sigma$  to separate them from the values of  $\nu$ , thus allowing an electronic filter to eliminate the disturbing components. Other methods will be discussed in the next section.

#### 4.0 Requirements for a practical FTS

A number of questions immediately arise when we wish to build an interferometer for a specific performance level. Here are some of the more important ones:

1. What are the long term mirror alignment stability requirements?
2. What are the sources of signal amplitude fluctuation during the recording and what measures can be taken to reduce or eliminate them?
3. What amplitude dynamic range and resolution will be required?
4. How accurately must the mirror position be known at the sample times and how can it be measured?
5. Are there problems unique to an imaging FTS using a detector array?

These questions will be discussed below along with some possible solutions. Again we must reiterate that there is a large volume of published literature addressing most of these issues in much greater detail than is presented here. Our objective here is to establish the starting point for a practical instrument design.

#### 4.1 Mirror alignment stability requirements

In the Michelson interferometer the fixed and moving mirrors are ideally optically parallel to each other, producing parallel waves after recombination at the beam splitter. If one of the mirrors is tilted relative to the other, either by a change in alignment of one of the mirrors or the beam splitter, the two waves will no longer be perfectly parallel and there will be a phase shift between the two beams as a function of the transverse position in the beams. To calculate the magnitude of this effect let us assume a mirror tilt angle,  $\alpha$ , and a beam width,  $Y$ . If the two waves emerge in phase at one edge of the beam the phase shift,  $\Delta\phi$ , at the other edge will be,

$$\Delta\phi = 4\pi\sigma\alpha Y. \quad (4.1)$$

For a rectangular aperture, with sides parallel to the direction of tilt, the effect of a  $2\pi$  phase shift from one edge of the aperture to the other would be to completely eliminate modulation of the beam, thus, we would like to keep the phase shift much smaller than this. It can be shown that the loss in signal for the rectangular aperture case is,

$$\text{loss} = 1 - \text{sinc}(2\pi\sigma\alpha Y) = 1 - \text{sinc}(\Delta\phi/2) \quad (4.2)$$

Let us arbitrarily choose a maximum allowable phase shift of  $0.6\pi$  radians at the largest wavenumber of interest,  $\sigma_u$ . (This will create about a 14% loss in amplitude of the interferogram according to equation 4.2). Then from equation 4.1,

$$\alpha_{\max} = 0.15/(\sigma_u Y) \quad (4.3)$$

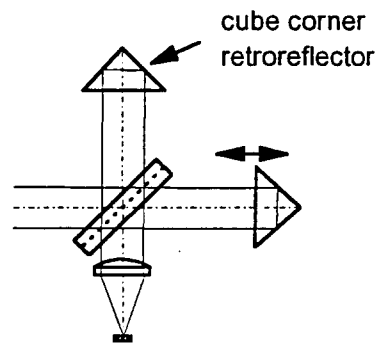
For example, let  $\sigma_u = 25,000 \text{ cm}^{-1}$  and  $Y = 1 \text{ cm}$ . Then  $\alpha_{\max} = 6 \times 10^{-6}$  radians = 1.2 arc seconds. This kind of alignment tolerance is difficult to maintain in practice, especially for the moving mirror, contributing to the lack of popularity of FT spectrometry at very large wavenumbers.

We should note that equation 4.2 predicts a wave number dependent responsivity as a function of mirror alignment. Thus, unless we can guarantee the stability of alignment, the FTS instrument must be frequently calibrated for responsivity as a function of wavelength. This can be accomplished in practice using a precision blackbody calibration source.

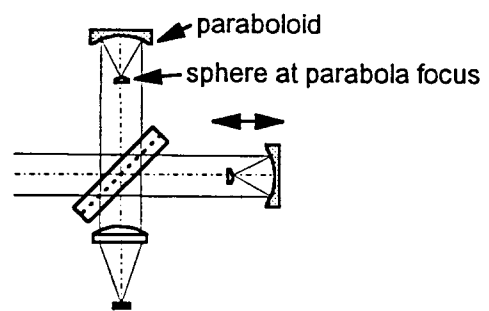
In a number of commercial laboratory instruments mirror alignment is maintained by using a computer driven two axis tilt servo on the stationary mirror. An automated alignment procedure is then performed on command wherein the signal from a test source is maximized by trial and error tilting of the mirror. This works good in the benign laboratory environment where vibration, temperature variation and other disturbances can be kept to a minimum. A more robust variation of this scheme might use an auxiliary interferometer to dynamically detect and correct the parallelism error. This greatly increases the number of peripheral electrical, optical and mechanical components.

Several passive solutions for alleviating the high accuracy requirement have been implemented by others using various retroreflector schemes. One such scheme is shown in Figure 4.1a. It replaces both the moving and fixed mirrors with cube corner reflectors. A cube corner reflector consists of three mutually orthogonal mirror surfaces. It has the property that any ray impinging on one mirror at such an angle that it is reflected from all three mirror surfaces will emerge parallel to the original ray but displaced from the original by twice the distance from the ray to the apex. A cube corner reflector can be made as a precision compact assembly, for example, using the surfaces of a glass prism. Maintaining good relative alignment of the prism facets is much easier than trying to maintain high precision in the entire interferometer consisting of separately mounted and aligned parts. This is especially true for the moving mirror. The use of a cube corner reflector eliminates much of the precision required of the mirror transport mechanism.

Another solution is to replace the flat mirrors with a combination parabola and sphere, as shown in Figure 4.1b. A ray approximately parallel to the axis of the parabola is reflected toward the parabola focus. It is again reflected back toward the parabola by a spherical mirror at the parabola focus. The ray emerging from the second reflection from the parabola is parallel to the incoming ray and, as in the case of the cube corner, it is displaced from the incoming ray by twice the distance to the parabola axis. The sphere curvature is chosen to be equal to the focal surface curvature of the parabola allowing the parallelism between the incoming and emerging rays to hold over a small range on input angles. We should point out, however, that off-axis aberrations in this optical scheme limit its use to relatively small fields of view. Its greatest advantage is at wave numbers where there is no suitable prism material. It may be somewhat easier to construct as a compact assembly than a corner cube made up of first surface mirrors.



a. Interferometer With Cube corner retroreflectors



b. Interferometer with parabola and sphere

Figure 4.1 Two schemes for Reducing Mirror Alignment sensitivity

One concern related to the reflector geometry is shear. The fact that in the retroreflective schemes described the return ray is not collinear with the entering ray can lead to shear between the two interfering beams emerging from the beam splitter in some cases. For example if the axis of symmetry of the two cube-corner assemblies or parabola/sphere assemblies is not optically colinear the two emerging rays will be displaced by twice the distance between the axes. (Shear also occurs for both flat mirrors and retroreflective mirrors for any ray entering the interferometer at an angle to the axis when the path distance between the two legs is not identical). Shear can reduce the interferometer output in two ways. The first is simply geometric; only the overlapping portions of the two emerging beams can interfere to produce the desired A.C. component of the detected signal. The second results from defects in the quality of the incoming wavefront. Shear in the interferometer places requirements on the quality of the optics used to form the incoming beam. Because of this the Michelson interferometer can be used only in cases where a high quality collimated wavefront can be provided, such as in the Earth viewing space telescope that we are primarily concerned with here. It could not be used, for example, in analyzing a scattering surface placed near the entrance aperture.

One result of shear produced by lateral motion of the moving mirror is that it may modulate the signal intensity producing some of the bad effects discussed in section 3.3. The effect, however, is a little different. Let us re-examine equation 3.7. Assume that the instrument is designed so that at maximum shear all the light from both paths through the interferometer is still collected by the detector. Then, fluctuations in shear will not affect the average value,  $A$ , but will modulate the coefficients,  $A_n$ . This means we can set the third term of equation 3.11 equal to zero, leaving only the fourth term, involving the products of coefficients  $A_n B_m$  as the effect of shear fluctuation.

#### 4.2 Eliminating signal fluctuation or its effects

In section 3.3 we found that signal fluctuation during the measurement period could add high amplitude spurious components to the apparent spectrum of the source and it also contributed a pseudo-random background noise equal to the fluctuation amplitude. For a FT spectrometer to successfully make high quality measurements it is imperative that we identify causes of actual or apparent signal fluctuation and to reduce the cause or its effect as much as possible. First let us list the various sources of signal amplitude fluctuation:

- a. source or propagation medium fluctuates causing variation at the input aperture of the instrument
- b. instrument line-of-sight varies while viewing structured scene
- c. velocity of moving mirror fluctuates causing variation in integration time of samples taken at constant position intervals.
- d. lateral fluctuation of moving mirror axis of a retroreflective mirror system causes varying amount of shear, modulating signal amplitude.

e. fluctuation in tilt angle of a flat moving mirror causes a wave number dependent modulation of the signal amplitude.

Obviously it is important to use whatever means is practical to reduce these causes as much as possible. For example an external source image stabilization mirror could be added to reduce item b; a good velocity feedback scheme could reduce item c; and good mechanical design of the drive mechanism could reduce items d and e. For the purposes of our discussion we will assume that these causes have been reduced as far as possible by direct means but that additional help is needed. Let us look at several additional things that can be done through further instrument design and data processing.

#### **4.2.1. Optimize mirror velocity**

As mentioned in section 3.3 one of the first things we should look at is whether we can separate the range of values of  $\sigma$  from those of  $v$  so that they are mutually exclusive. Then we can use an electronic filter in the signal output to eliminate the fluctuation components. This may require driving the mirror faster or slower, which, of course, is not always possible. Changing the mirror velocity will always change the values of  $\sigma$  relative to the values of  $v$  in cases a and b. In cases d and e the cause of fluctuation may still be external, such as vibration, so this first method could still be effective. Other causes could produce fluctuations with frequencies directly proportional to the mirror velocity, for example, position dependent friction in the drive or deviations in straightness of the track carrying the mirror. In these cases there is no improvement from a change in mirror velocity.

#### **4.2.2 Normalize integration**

An improvement which is applicable only to case c. is to detect the integration time differences and use the information to normalize the signal amplitude. In case c we have made the assumption that some means is used to sample and reset an integrator at exact position intervals of the driven mirror. For now we are only concerned with the effects of integration time variations. A simple way to eliminate this error, electronically is to use an auxiliary circuit to integrate a reference voltage, with the sample and reset being triggered from the same source that triggers the real signal interval. The ratio of this auxiliary integrator output with the signal integrator output produces a signal with amplitude independent of the integration time. A way to accomplish the same thing digitally is to use a high speed clock to measure the time interval between samples. Dividing by this time will then normalize the output. In practice this must all be done with caution since the second integrator, or the timer, could add random noise to the output. Whether or not there is a net improvement in the measurement accuracy depends on the magnitude of the velocity fluctuations.

#### **4.2.3 Pre-sample the total input amplitude**

By placing a beam splitter just in front of the input aperture of the interferometer the input signal can be sampled and recorded along with the interferogram. The ratio of the

interferometer output to this reference signal should then yield a signal free from fluctuation. Again, if these samples are taken as described in 4.2.2, the effect of mirror velocity variations would also be removed. This looks like a powerful technique but there are a few pitfalls to watch out for. These are listed below:

1. A beam splitter at the input will reduce the input amplitude available to the interferometer, thereby reducing the signal to noise ratio. In order to maintain equal signal to noise ratio in the sampler and interferometer outputs an ideal beam splitter must remove 1/3 of the incoming light.
2. The pre-sample will also contain noise which, when ratioed with the interferometer signal, increases the total noise.
3. This technique does nothing for cases d and e.
4. For this technique to be effective we must assume that the fluctuations of input light amplitude are independent of wave number. That is, we must assume that the  $A_n$  coefficients are not fluctuating relative to one another but that the modulation affects them all in the same proportion. This is usually only approximately true in practice. For example atmosphere caused scintillation is often wave number dependent. If the fluctuations were coming from a changing current driving an incandescent lamp the amplitude changes would also be accompanied by a color temperature change. If the fluctuation is due to line-of-sight variation to a structured scene the condition could be badly violated since different portions of the scene could contain very different color mixes.

#### 4.2.4 Dual output subtraction

In the Michelson interferometer there are always two output beams. When flat mirrors are used in the two legs of the interferometer one of these output beams is coaxial with the input beam and cannot be accessed. Figure 4.2 shows an interferometer using corner reflectors for the two mirrors. The input beam is displaced from the center allowing both output beams to be collected without obstructing the input. If the beam splitter dividing the two arms of the interferometer is ideal the amplitudes of the two output beams will be identical but the oscillations due to light interference over the two paths will be exactly 180 degrees out of phase. If we subtract one output from the other the resultant signal will not contain the large D.C. term or any products of this term with external fluctuation terms. The A.C. terms will have twice the amplitude. Re-examining equation 3.11 we are left only with the second and fourth terms, i.e. the real source spectrum with coefficients  $A_n$ , and the product spectrum with coefficients  $A_n B_m$ .

This also appears to be a powerful technique. The fact that both output beams are used increases the signal-to-noise ratio whereas the previous ratioing scheme reduced it. Within the ideal beam splitter assumption, the cancellation does not depend on there being any correlation of the fluctuations over the wave number range, since the cancellation is done on a sample by sample basis. A few negative aspects of this scheme are listed below:

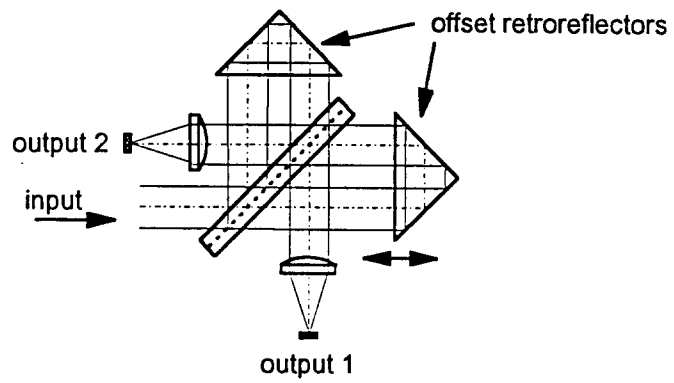


Figure 4.2 Interferometer with Offset Retroreflectors

1. Unlike the ratioing scheme, this subtraction scheme does not get rid of all the noise terms generated by fluctuation of the input intensity.
2. This scheme does nothing for cases c, d, and e.
3. In order to gain access to the second output corner reflectors need to be used off center, more than doubling the size of the beam splitter and reflector surfaces.

As we have seen in this section it is possible, through the use of auxiliary signals generated by the interferometer, to greatly reduce the effect of input signal fluctuations. The most effective method will depend on the nature of the fluctuations, for example, whether they are wave number dependent or whether they are generated internally or externally.

### 4.3 Amplitude dynamic range and amplitude resolution

One of the practical difficulties with FT spectrometry compared to other techniques is that the amplitude dynamic range of the interferogram is greatly increased over that of the expected range of signal intensities (Mertz 1965, pp. 27-29; Hirschfeld 1979). This leads to a loss of precision when signals are digitized by an A/D converter. To illustrate this we can look again at equation 3.7 where  $A$  is the sum of all the spectral component coefficients,  $A_n$ . For a spectrum of  $N$  components the value of  $A$  will be  $N$  times the value of the average coefficient,  $A_{avg}$ . The peak value,  $I_{peak}$ , of an interferogram having no phase dispersion will be twice this value, occurring at the zero path difference position of the moving mirror. Thus we can write,

$$I_{peak} = 2 N A_{avg} \quad (4.4)$$

Let,  $j$ , be the number of bits of A/D converter resolution. If we adjust the gain of the signal before the converter so that the peak signal just covers the range of the converter the amplitude,  $I_{lsb}$ , of the least significant bit will be,

$$I_{lsb} = I_{peak} / 2^j \quad (4.5)$$

We then define the rms noise in the interferogram due to digitization as,

$$\text{digitization rms noise} = 1/3^{1/2} I_{lsb} \quad (4.6)$$

where the factor,  $1/3^{1/2}$ , is simply the conversion from the rectangular digitizer steps to an equivalent rms value. The digitization related peak signal to rms noise ratio in the original interferogram is then,

$$\text{SNR}_{int} = 3^{1/2} 2^j \quad (4.7)$$

which is obtained by solving equation 4.5 for  $I_{peak}$  and then dividing by equation 4.6. We can now ask the question, what is the average signal to rms noise ratio in the Fourier

transformed spectrum. By substituting for  $I_{\text{peak}}$  in equation 4.5 from 4.4 and solving for  $A_{\text{avg}}$ , we get,

$$A_{\text{avg}} = I_{\text{lsb}} 2^j / (2N). \quad (4.8)$$

Dividing this by equation 4.6 gives the SNR of the average spectral component, but the interferogram is made up of a large number of measurements. If we assume that  $N$  is the number of resolvable elements in the measured spectrum then for a full two sided interferogram there must be  $4N$  measurements (see equation 2.7). This would be expected to improve the signal to noise ratio by a factor of  $2N^{1/2}$ . Combining this with the ratio of equation 4.8 to 4.6 we see that the signal to rms digitization noise for the average spectral component of amplitude  $A_{\text{avg}}$  in the Fourier transformed spectrum is,

$$\text{SNR}_{\text{FT}} = (3/N)^{1/2} 2^j \quad (4.9)$$

Comparing equation 4.9 with 4.7 we see that the SNR due to digitization in the transformed spectrum is  $N^{1/2}$  times worse than in the original interferogram.

We can easily extend this result to compare the FT interferometer with a direct spectral measurement spectrometer such as a grating based instrument. To do so we need to define a few more quantities. Let  $A_m$  be the largest amplitude spectral component and  $r = A_{\text{avg}}/A_m$ . For the grating instrument we set the A/D range to be equal to  $A_m$  just like we set it equal to  $I_{\text{peak}}$  in the FT instrument. Following the same procedure as described for the FT instrument we get,

$$\text{SNR}_{\text{grat}} = 3^{1/2} 2^j r \quad (4.10)$$

$\text{SNR}_{\text{grat}}$  is the signal to digitization noise for the average spectral component  $A_n$  as measured by a grating instrument, thus, it is directly comparable with equation 4.9. Doing so, we get,

$$\text{SNR}_{\text{grat}}/\text{SNR}_{\text{FT}} = N^{1/2} r \quad (4.11)$$

As a brief example, let us look at a wave number of  $12,000 \text{ cm}^{-1}$  with a resolution of  $1 \text{ cm}^{-1}$  ( $N = 12,000$ ). From equation 4.9 the SNR of the average Fourier transformed component is  $.0158 \times 2^j$ . If we desire a 0.1% resolution we must have a SNR of 1000. Solving for  $j$  we find that we must use at least a 16 bit encoder. To compare this with a grating instrument we need to assign a value to  $r$ . If we are looking at weak absorption spectra in a continuum the value of  $r$  could be close to 1. We will assign a value of 0.5. Using equation 4.10 and solving for  $j$  we find that the grating instrument achieves the same precision with slightly over 10 bits.

In the examples above the A/D converter range was set equal to the largest amplitude seen in a single record. In practice we would of course have to allow for variations in source amplitude, setting the gain before the A/D converter to cover the maximum signal

expected. In the case of an imaging system the variation from pixel to pixel and scene to scene could be quite large. Some kind of automatic gain ranging could be required in a field instrument. Even so it is doubtful that it will always be set at optimum for a given record. In that case we must accept an even greater loss of accuracy.

Whether or not the loss of resolution is a problem depends on the required measurement accuracy, the required measurement speed and the nature of the spectrum being measured. A/D converters can be built with a larger number of bits of resolution to recover the precision but speed or power are sacrificed. Maximum speed and the minimum number of converter bits becomes a critical issue when dealing with detector arrays, especially when the array itself may have a very limited dynamic range.

One way to deal with this problem is to reduce the interferogram amplitude dynamic range by introducing a phase dispersing component in the optical path of one leg of the interferometer. This method was first suggested by Mertz (1965, pp. 29-30), who called the method, "chirping". In a perfect interferometer the equal path length position is the same for every wave number creating the very large peak at the center of a symmetrical interferogram. If a dispersive material, such as a piece of glass, were introduced into one leg of the interferometer and not the other the optical path length through the material would vary as a function of wave number. The moving mirror position for equal path length in the two arms of the interferometer would then vary as a function of wave number and there would not be a single position where all wave numbers are in phase. By choosing the dispersion and thickness of the material the large central maximum of the interferogram could be spread out over any desired distance, greatly reducing the central peak amplitude. A phase correction algorithm must then be applied to the data when it is Fourier transformed. Several algorithms have been developed (Forman 1966; Mertz 1965, p. 42; Wolf 1967, pp 291-295). Some require no knowledge of the actual phase dispersion while others use an auxiliary measurement to determine the actual phase dispersion, taking advantage of the fact that dispersion in most materials is a smooth function. One additional advantage of using certain phase correcting algorithms is that any point on the interferogram may be used as the center, making it unnecessary to use an auxiliary optical means to locate the exact center.

A few other techniques for dealing with the large dynamic range can be found in commercial instruments. The first is gain ranging. If we look at an interferogram (without the phase dispersing element described above) of a continuum we see a very large central peak, rapidly falling to smaller values as the distance from center increases. Thus, if the gain is reduced before the ADC for some number of samples on each side of the peak the effective  $j$  can be increased. Commercial laboratory instruments typically get 2 to 3 additional bits of accuracy with this technique. For best results, though, it requires some pre-knowledge of the signal being observed in order to set the sample numbers at which the switching is to occur. The other powerful technique is to average a large number of interferograms of the same spectrum. The SNR is then increased by the square root of this number assuming that other random noise in the system is large enough to cause the digitization noise to be uncorrelated between successive interferograms. If the luxury of using multiple measurements is available it could, of course, also be used with a grating

instrument to help overcome its throughput disadvantage discussed in section 3.2. These factors should be seriously considered before a FT instrument is chosen for a particular measurement scenario.

#### 4.4 Sampling interval accuracy requirements

In section 2.2 we derived requirements for the maximum allowable mirror travel intervals for sampling the interferogram amplitude. In this section we want to look briefly at the effect of errors in these sampling intervals on the Fourier transform in order to establish requirements for a measurement system.

We define sampling interval error as any deviation from strictly equidistant spacing of the samples in terms of the moving mirror position. Intuitively we would expect problems if there is error in the sampling interval since it is the basic unit of measure of wave number for the instrument. There are two possible effects produced by sampling interval fluctuation. One is amplitude modulation and the other is phase modulation. Amplitude modulation can result from a fluctuation in the time between samples. For example, if we assume that the mirror is traveling at a constant velocity any variation in the sampling interval will also result in a variation in the time between samples. As discussed in section 4.2.2 this would cause an amplitude fluctuation in the signal as measured by a reset integrator, (or any electrical bandwidth limited system). The effect of this amplitude fluctuation was discussed in section 3.3. The amplitude and phase modulation are not always present together. As an example of phase modulation without amplitude modulation imagine a system in which samples are taken at strictly equal time intervals. This is sometimes demanded by the electronics, for example, a delta-sigma A/D converter. Now any fluctuation in the mirror velocity will result in a phase modulation of the signal since the sampling intervals are not constant in terms of mirror position. It is important to realize that the amplitude and phase modulation components are two separate phenomena and may need to be dealt with separately.

In section 3.3 we derived equation 3.11 showing the effects of amplitude modulation on the interferogram signal. In a similar manner we can derive the effect of phase modulation. If, for a given measurement of the interferogram there is an error,  $\epsilon$ , in the  $x$  position at the time of measurement then the actual measurement is taken at position  $x + \epsilon$ . Starting with equation 3.7 we insert this error, giving,

$$\begin{aligned} I_{\text{sig}}(x) &= A + \sum^N A_n \text{Cos}[4\pi(x + \epsilon)\sigma_n] \\ &= A + \sum^N A_n \text{Cos}(4\pi x \sigma_n + 4\pi \epsilon \sigma_n) \end{aligned} \quad (4.12)$$

For simplicity let us consider what happens when  $\epsilon$  varies periodically, taking the form, of a single frequency sinusoid of equivalent wave number,  $\nu$ . Then,

$$\epsilon(x) = \Delta x \text{Sin}(4\pi x \nu). \quad (4.13)$$

$\Delta x$  is just the peak deviation of  $x$  from its correct position. This is a practical case which might arise when taking data at constant time intervals and there is a mechanical disturbance which excites a natural resonant frequency in the mirror drive system, causing its velocity to vary in a sinusoidal manner. We can now substitute for  $\epsilon(x)$  from equation 4.13 in 4.12. Each of the  $N$  components of the resulting equation can be expanded as an infinite series of Bessel functions of the first kind. In general, there will be components at each of the original wave numbers,  $\sigma_n$ , as well as an infinite series of components at wave numbers,  $\sigma_n + \nu$ ,  $\sigma_n - \nu$ ,  $\sigma_n + 2\nu$ ,  $\sigma_n - 2\nu$ ,  $\sigma_n + m\nu$ , etc. Let,

$$C = 4\pi\sigma_n\Delta x. \quad (4.14)$$

Then the amplitude of the component at wave number,  $\sigma_n + m\nu$ , will be,  $A_n J_m(C)$ , where,  $J_m(C)$ , is the  $m$ th order Bessel function. For  $C \ll 1$  the dominant terms will be  $J_0$  and  $J_1$ , in which case we can make the approximation,  $J_0 = 1 - C^2/4$ ,  $J_1 = C/2$ , and set the higher order terms equal to zero. For example, let  $C = 0.1$ , then  $J_0 = .9975$ ,  $J_1 = .0499$ , and  $J_2 = .00125$ .

As an example, it is interesting to look at what kind of periodic error function amplitude will give us an error of 0.2% in the amplitude of a spectral line. From equation 4.14 it is obvious that the worst case occurs at the largest wave number being measured, so, for this example we will choose a value of,  $\sigma_n = 25,000 \text{ cm}^{-1}$ . If we look at just the original frequency component, with an amplitude represented by  $J_0$ , we can set  $C^2/4 = 0.002$ . substituting for  $C$  in equation 4.13 and solving for  $\Delta x$ , we get,  $\Delta x = 2.8 \times 10^{-7} \text{ cm}$ . We can also look at the error produced when one of the spurious components is added to one of the real spectral components. Using the approximation,  $J_1 = C/2$  and setting  $J_1 = 0.002$  we find an allowable value of  $\Delta x = 1.3 \times 10^{-8} \text{ cm}$ . These errors should be compared to the sampling interval distance itself. From equation 2.5 we will need a sampling interval of  $10^{-5} \text{ cm}$ , thus, the allowable error is about 0.13% of the interval. This example points out the interesting fact that the percent amplitude error from a single spurious component is roughly equal to the peak percent error in the sampling position. Clearly, If we wish to make precision measurements of relative spectral line amplitudes we must keep the sampling position error very low.

#### 4.5 Methods of sample interval generation

Various methods have been used for generating precise sampling intervals. The most common device used in modern laboratory instruments is an auxiliary interferometer based on a HeNe gas laser. The collimated laser light is made to travel nearly the same path through the spectrometer as the external light being measured but offset so that it will not fall on the detector used to measure the external light. An auxiliary detector in the laser light path then receives only the light from the laser, producing a pure sinusoidal output as the mirror is moved. Before the HeNe laser became common, spectrometers often used a filtered neon lamp output for the reference. More recently, the output of a collimated laser diode has been used. The laser diode reference will be examined more closely in section 5 when we discuss specific implementation. The advantage of the laser is that it has the potential for producing a high amplitude signal with very low noise. Other

schemes can be found in the literature which use capacitance or inductance change, or which use external optical or inductive based periodic scales attached to the mirror shaft. Many of these non-laser based schemes have been used successfully in a long wave infrared instrument but published accuracies fall short of the few nanometers we desire for a visible/UV instrument.

Let us look a little closer at the laser interferometer based sample interval generation scheme. In the typical laboratory instrument a zero crossing detector is used to produce a pulse at the exact point of transition of the sine wave through a point near zero amplitude. Since there is always a small amount of unpredictable offset in any electronic amplifier circuit the exact trigger point may be slightly above or below the true zero. If the trigger point is not exactly zero and if the laser signal fluctuates or there is noise in the amplifier circuit there will be some fluctuation in the spacing of the sample pulses. If we want to use transitions in both positive and negative directions to generate sample pulses we must also be concerned that the two circuits used will have different trigger points causing the pulses to be slightly unevenly spaced. In spite of these potential errors the zero crossing triggered sampling scheme is probably the most accurate we can generate. The most serious problem with this sampling pulse generating scheme is that, at best, sampling pulses are available only twice per cycle of the laser interferometer signal. This means the measurement short wavelength cutoff for the instrument will be equal to the laser wavelength. This is a serious problem if we wish to extend measurements into the near UV region. The shortest HeNe laser wavelength is 632.8 nm ( $15,803 \text{ cm}^{-1}$ ) and a single frequency laser diode wavelength is even higher, around 800 nm ( $12,500 \text{ cm}^{-1}$ ). Clearly another sampling scheme will have to be found. Although there may be a number of schemes worth considering we will look at just four here.

1. Velocity stabilization. In this scheme the laser generated pulses are not used directly for signal sampling but are used as a tachometer signal to precisely control the velocity of the mirror servo. If the velocity can be kept sufficiently constant the signal samples can be taken at equal time intervals. This has the advantage of eliminating electronic system phase errors and facilitates use of digitizing schemes which demand equal time interval samples. It has the disadvantage that it places possibly unachievable requirements on the mirror velocity servo system.

2. Phase locked loop frequency multiplier. The problem with scheme 1 is that it requires that a large physical mass, the mirror system, be precisely controlled. In a vibration isolated laboratory environment this might be achievable but in a space instrument subject to severe weight constraints and vibration from various sources on the platform it is less certain. One way of working around this is to take the problem out of the mechanical domain and place it in the electrical domain. In this scheme we use reasonable means to drive the mirror at a near constant velocity. We then use the laser generated pulses to lock a phase locked loop oscillator operating at some multiple of the laser pulse rate. To aid tracking of the oscillator the loop filter is made to match the mechanical characteristics of the mirror and drive system. This system will provide accurate intermediate sample pulses as long as the frequency of any drive system oscillations is low compared to the laser generated pulse frequency. The main

disadvantage of this scheme is that samples are not at strictly equal time intervals, meaning that a digitization system requiring equal time intervals will not work. Unequal time intervals will also require correction of the resulting amplitude modulation as discussed in section 4.2.

3. Interpolation. This scheme combines the best features of 1 and 2. Samples are taken at equal time intervals and the mirror is driven at a reasonably, but not strictly, constant speed. The exact laser signal zero crossing times are also recorded. A non-linear interpolation algorithm is then applied to the zero crossing time data to estimate the mirror position at the equal spaced sample times. A second interpolation algorithm is then applied to the sampled interferogram to obtain accurate amplitude estimates at the desired equal mirror position intervals. This is a truly modern scheme because it avoids reliance on a precision drive mechanism and places the problem into a digital computer based digital filter. At least one successful implementation of this concept has been recently reported (Brault 1996).

4. More interpolation. One disadvantage of the third scheme is that a high speed clock is needed to accurately measure the zero crossing periods. For example, if we drive the mirror so that zero crossings of the laser reference occur at a 10 KHz rate and we desire a quantization error of no greater than 1 part in  $10^4$  we will then need a clock frequency of 100 MHz. If we carry the concept of the third scheme a little further we can eliminate the zero crossing detector and the need for a high speed clock by using an A/D converter to sample and record the amplitude of the laser generated sinusoid at the same time as the external signal is being sampled or at a known, fixed, time difference. A digital filter based interpolation of this data will then yield an accurate estimate of the zero crossing times. This scheme has the disadvantage of requiring an additional A/D converter and additional computational effort but potentially offers greater accuracy than just measuring zero crossing times since a number of measurements of the signal can be made during a single cycle of the sinusoid. Since interpolation is involved in both the reference signal and external signal both may benefit by more frequent sampling than that strictly required by the Nyquist criterion. The optimum number of reference samples per cycle will depend on the nature of any disturbances and the allowable A/D converter speed.

To test the fourth concept a simple computer simulation was performed. A sinusoid was amplitude modulated, producing 40% amplitude variations at a modulating frequency of about 0.125 of the test sinusoid. The signal was then sampled at intervals of approximately 0.3 period (Nyquist rate would be 0.5 period). A sinc interpolation was then done using a Hamming window of various lengths. A number of interpolated points were generated and a linear interpolation was done to estimate the zero crossing times using the two points nearest the zero crossing. With a 16 element window and 10 interpolated points between samples the maximum zero crossing time error observed was  $4 \times 10^{-4}$  times the period of the sinusoid. Using a larger window size or smaller sample period any desired accuracy could be achieved in the simulation. Phase modulation was not simulated but the results are expected to be similar.

Of the four schemes the last two provide the best features and most likely chance of successful implementation. It is not clear which of these would yield the most accurate results or be the easiest to implement in practice.

In addition to the generation of sampling pulses at precise intervals it is often desirable to keep track of the absolute mirror position. The need for an absolute position reference arises when we want to take a large number of successive interferograms and add them together to improve the signal-to-noise ratio before performing the Fourier transform. If the transform is performed on individual scans no absolute reference is necessary although it might still be desirable as an aid in calculating the phase correction for a series of scans. Relative position, in increments of the laser signal zero crossings, can be obtained by simply counting the number of zero crossings, starting from some absolute position fiducial. The simplest fiducial is a precision mechanical stop at or slightly beyond one end of the measurement range of mirror travel. Another method is to use an auxiliary white light source, such as an incandescent lamp, traveling over a third path through the interferometer, to its own detector. The large central peak created by this source can then be used to record the sample count at the center. The only restriction is that the path used for the white light source must be phase compensated, i.e. it must have the same phase dispersion in both arms. One disadvantage of using the incandescent lamp is that a path through the interferometer must be found for it which does not interfere with the signal or reference laser path. Another alternative is to avoid the necessity for an absolute position fiducial by always keeping track of the incremental position count in both directions of mirror travel. One method for doing this will be discussed in section 5.

#### **4.6 Aspects unique to an imaging FT spectrometer**

There are some unique aspects to using an imaging detector array in a FT spectrometer that bear looking at briefly. Several of these are discussed here:

##### **4.6.1 Wider total field-of-view potential**

In section 2.4 we found that the allowable field-of-view of a single detector element was limited by the desired resolution divided by the wave number. In an instrument consisting of many detector elements this relationship is applied to each element separately, thus, we have the potential for looking at a larger total field-of-view. In order to accommodate a large field-of-view it is desirable to keep path lengths through the instrument as short as possible in order to minimize component sizes. This could dictate the optical configuration. For example, it might force the use of flat mirrors instead of corner reflectors.

##### **4.6.2 Angle dependent processing required**

Each element of a detector array looks through the optical system at a different angle. This means that all path differences must be divided by the cosine of the angle between the moving mirror axis and the line-of-sight angle of each detector. This is easily handled in the data processing since each of the angles is fixed and easily calculated.

### 4.6.3 Array readout scheme accommodation

Several readout schemes can be found in practice. Some systems use a block transfer method in which the array integrates the photon input for a specific time, at the end of which the array is temporarily disabled, read out into an auxiliary array, and reset. With this scheme every pixel integrates over exactly the same mirror travel distance. In theory, this type of array could be read out at unequal time intervals, triggered by zero crossings of the reference interferometer signal. At the other extreme is the more popular readout method in which each pixel is read out and reset in sequence. In this case, although the integration times are identical for each pixel, the moving mirror starting and ending positions are different. For this kind of array it is imperative that the array be read out using a fixed clock rate and that the mirror position be known at any time, not just at the reference interferometer zero crossing times.

### 4.6.4 Limited array dynamic range

The large amplitude dynamic range of interferograms was discussed in section 4.3. This can create a serious problem, especially for low cost, mass produced, CCD silicon detector arrays, which may have been designed to produce a suitable television image under controlled lighting conditions. Some of these may have as few as 8 bits of useful dynamic range. Even with the addition of unbalanced dispersion to reduce dynamic range it may be necessary to design special arrays with large charge storage capacitance for use in an interferometer application.

### 4.6.5 Data storage and processing requirements

A simple example will make the point here. Let us look at the storage requirements for one double sided interferometer scan using a 256 x 256 element array, amplitude digitized to 16 bits, a spectral resolution of  $1 \text{ cm}^{-1}$  and a maximum wave number of  $25,000 \text{ cm}^{-1}$ . About  $2^{17}$  samples must be taken from each pixel. Adding it all up we need about  $1.4 \times 10^{11}$  bits of storage for each image. In a practical scenario this data must be collected in a relatively short period of time in order to preserve the geometry and spectral characteristics of a dynamic scene. It is obvious that the data rate and volume could easily go beyond the capabilities of any reasonable computer system. Methods of reducing data storage requirements are one of the greatest challenges to building a practical imaging FT spectrometer of moderate resolution for space applications. One possibility is to use direct digital filtering of the data as it comes in to look at specific spectral lines or regions of interest for a particular application. This might avoid having to store an entire frame of data before it is processed and would greatly reduce the post-processing data storage requirement. The penalty is that a large amount of real time computation must be done. This is further complicated by the possible need to perform phase correction and sampling time corrections. A separate study of data processing methods and storage requirements is needed in order to determine the limits achievable. This is outside the scope of the present study.

## 5.0 The SWIFTS breadboard instrument

A breadboard instrument was constructed to allow us to evaluate a number of aspects of practical interferometer design for space applications. The breadboard was not designed to be a prototype for a flight system but, rather, to act as a platform for trying out ideas and evaluating them. Some of the specifics of this design will be discussed here. First we will look at the design goals and then at several of the components of the system.

### 5.1 Design goals

Some of the major design goals are listed below, not necessarily in the order of importance:

1. Operation over the entire silicon detector region of approximately 0.4 to 1.1 microns ( $9,090$  to  $25,000$   $\text{cm}^{-1}$ ).
2. minimum mirror travel distance of 1 cm, allowing a two sided interferogram with an unapodized resolution of  $1$   $\text{cm}^{-1}$ .
3. no precision adjustments required
4. 1 cm diameter entrance aperture
5. no lubricated components in the mirror drive system
6. a simple launch lock method built into the drive mechanism
7. a mirror position measuring means capable of efficient, long life operation in space
8. a means of evaluating the relative merits of various methods for dealing with input signal amplitude fluctuation
9. a means of driving the moving mirror in various ways (i.e. open loop ramp, velocity feedback, etc.) in order to be able to assess the adequacy of various data processing algorithms.
10. field of view through system adequate for the testing of a small detector array

### 5.2 Components of the primary optical system

A Michelson interferometer with cube corner reflectors was implemented. A simplified schematic diagram of the primary light path is shown in Figure 5.1. Although cube corner mirrors were used they are shown as V mirrors to be able to represent the system in two dimensions. The incoming light first encounters an Inconel beam splitter, consisting of a thin Inconel film vacuum deposited on a flat glass plate. This is used to split off a sample of the incoming light for source amplitude fluctuation compensation experiments.

The best place for the entrance pupil defining aperture is dependent on the relative size of available components. In the SWIFTS breadboard a single 1.8 cm diameter aperture was placed just after the sampling beam splitter and before the interferometer beam splitter. Since the path length through the interferometer to the detector is about 40 cm from this point only a relatively narrow field-of-view gets through without vignetting. An identical aperture, equidistant from the sampling beam splitter in the reflected light leg, is also necessary to insure that the sampling detector will see the same light seen by the interferometer detector.

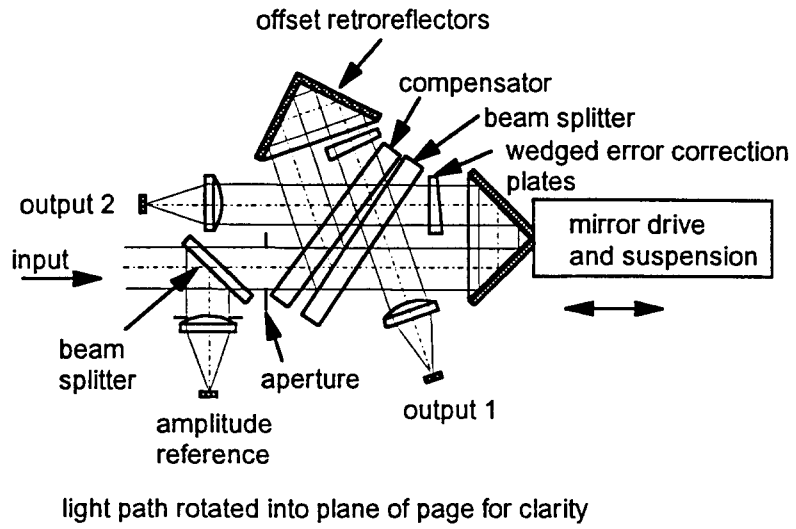


Figure 5.1 Primary Optical Path of the SWIFTS Breadboard

The light next encounters a phase compensator and beam splitter. These are two identical pieces of glass except that one surface of one of them is coated with vacuum deposited Inconel. The other surfaces are single layer anti-reflection coated. Inconel was used for both beam splitters because its transmittance and reflectance are nearly constant over the spectral range of interest. Inconel would be a poor choice for a flight instrument because it has very low efficiency. A beam splitter made of this material, intended to reflect and transmit equal amounts of light, will only reflect about 30% and transmit 30%. About 40% of the light is absorbed in the metal film. A more efficient beam splitter would use multi-layer dielectric coatings which can approach 100% efficiency (50% transmitted and 50% reflected). Because of the high cost and long development time for a more efficient, wide bandwidth beam splitter the lower cost, more expedient choice was made. None of the experiment goals were concerned with efficiency. In the breadboard the phase compensator plate is mounted with about a 2 mm gap between it and the beam splitter surface. A slight wedge angle between these two plates reduces the effect of multiple reflections. If the phase compensator plate were made slightly thicker or thinner than the beam splitter plate this wedge angle could be fine tuned to create a symmetrical interferogram if this was desired. Light passes through the beam splitter toward the moving cube corner retroreflector and reflects from the beam splitter towards the fixed cube corner retroreflector. The reflected light makes about a 70 degree angle with the incoming light rather than 90 degrees in order to allowing a slight reduction in the size of the compensator and beam splitter.

The next components in the light path are the cube corner retroreflectors. The reflectors used in the breadboard are made up of three individual front surface mirrors permanently glued into a precision aluminum mount (Newport model BBR2.5-0.5). While we would have preferred a cube corner reflector made from a single piece of glass no off-the-shelf item could be found with the right size and quality. The Newport assemblies have a clear aperture 2.5 inches in diameter, 0.5 arc second parallelism between incoming and reflected beams, and 1/3 wave distortion in the visible over the entire aperture. The large size of these components is necessary to accommodate a displaced axis. In order to allow separation of the incoming and outgoing beam and to allow an isolated path for the laser interferometer, the cube corner axis of symmetry is placed about 0.85 inches off of the axis of the incoming beam. Figure 5.2 shows a view looking into the cube corner reflector along the axis of symmetry. In addition to the three lines dividing the three mirror intersections we see three other reflected intersections, dividing the mirror into 6 equal sectors. In order to minimize wavefront distortion the mirrors were oriented in such a way that the entire beam diameter fits within one of these sectors. A beam going into one of these sectors will be reflected out of the sector on the opposite side of the axis. Thus, by properly placing the incoming beams we can accommodate three separate beams. One of these is the incoming light; another is the reference laser; and a third could be an internal white light source used for determining the center of the interferogram. This third beam was not implemented in the SWIFTS breadboard.

Keeping the beam of light all within one sector is costly in terms of the required mirror sizes. It does have the advantage, though, of allowing correction of construction errors in the angles between the cube corner reflector mirrors. For example, if we assume that the

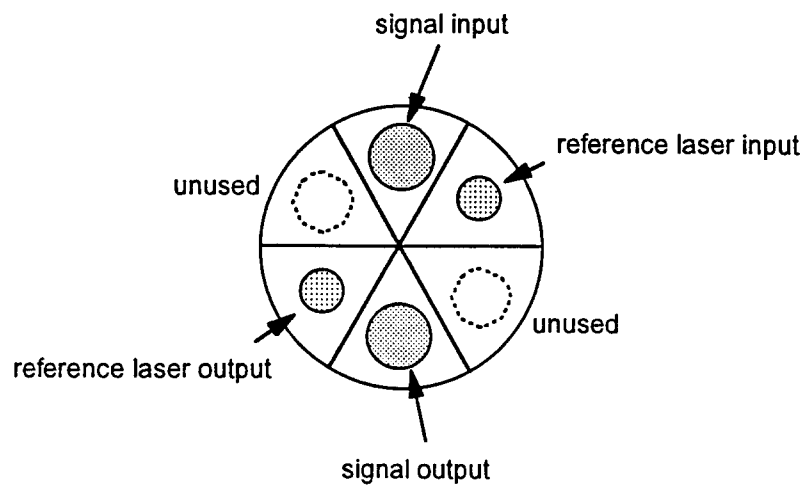


Figure 5.2 View Looking Into Retroreflector Axis of Symmetry

three mirrors making up the cube corner are perfectly flat but that they are not exactly mutually perpendicular, then the only error in a beam reflected by the system is that the output will not be perfectly parallel to the input. In practice we can correct this error in two ways. One is to rotate either the fixed or moving mirror assembly about its axis to see which of the three unique positions gives the smallest non-parallelism between rays entering the detector system from the two interferometer paths. In other words, we can look for a position in which errors in the two assemblies tend to cancel each other. The second way is to insert identical but slightly wedged glass plate into the path of each branch of the interferometer. If the maximum angle deviation through the plates is greater than the cube corner mirror error a position can be found by rotating the plates where the errors will be canceled. If the wedge angles are made only slightly larger than is required to correct the error the required precision of adjustment is very coarse. These wedged plates were not required on the SWIFTS breadboard; the cube corner reflectors, as received, were accurate enough.

The last component in the optical system is a lens used to focus the recombined light onto a detector. For an imaging system this lens needs to have a quality in keeping with the desired image resolution but for the first phase of the SWIFTS breadboard testing a single element lens of about 35 mm focal length was used in conjunction with a 0.1 inch diameter single element detector (EG&G SGD-100). The lens, detector, and preamplifier were built into a single pre-aligned assembly. A total of three identical assemblies were used, one for the primary signal receiver, one for the laser reference receiver, and one for the auxiliary signal receiver. The auxiliary signal receiver is used for signal fluctuation cancellation experiments. It is placed in one of two positions, either at the output of the sampling beam splitter or at the second signal output of the interferometer (see Figure 5.1).

### **5.3 Moving mirror suspension and drive system**

The moving mirror was suspended by a pair of radially symmetrical flexure springs and was driven by a "voice coil" type actuator. A sketch of this system is shown in Figure 5.3 with a few dimensions shown. This assembly is much larger than would be desirable for a practical flight system but serves as a starting point for a more sophisticated design.

A conceptual drawing of two flexure spring designs is shown in Figures 5.4 a and b. A simple diaphragm spring is shown in Figure 5.4a. This is not the one finally used in the SWIFTS breadboard but serves better to illustrate the principle. It consists of a thin metal disk with rigid mounting surfaces in the center and at the perimeter. Three spirals are cut into the disk going from center to edge. These cuts reduce the axial (perpendicular to the surface) stiffness of the diaphragm, while maintaining a high radial stiffness. A pair of these springs is separated by some distance with the perimeters mounted to fixed rigid surfaces. A shaft attached to the two centers is then able to move along its axis with the application of a small force, but a much larger force is required to displace the shaft laterally. Flexure spring type mounts have been used in many applications. The advantage of a radially symmetrical system like the diaphragm spring in our application is that the shaft moves only axially and is not displaced laterally as the shaft moves. There are two

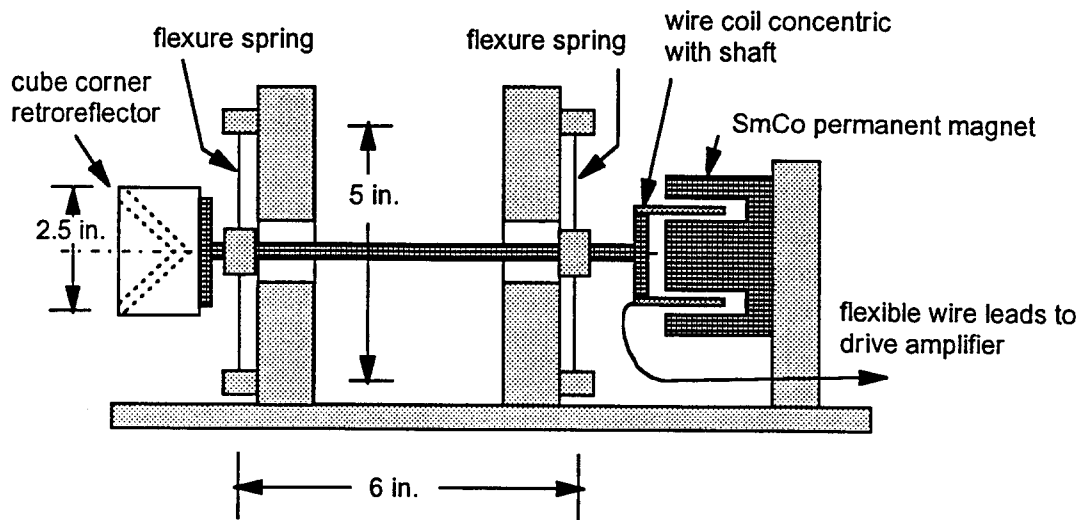


Figure 5.3 Moving mirror Drive and Suspension System

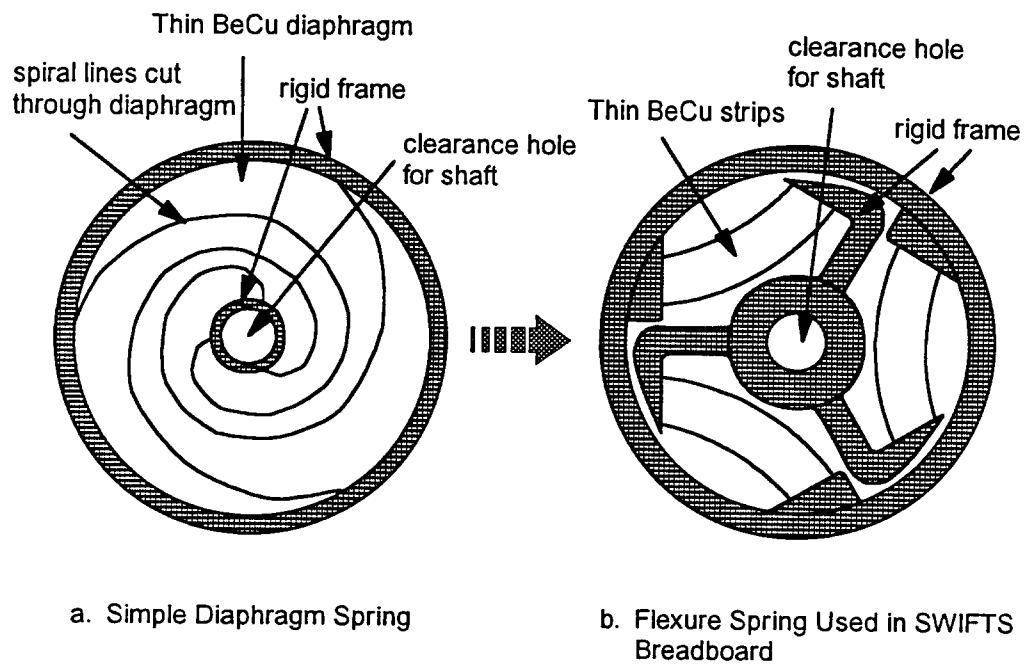


Figure 5.4 Flexure spring designs

disadvantages to the spring arrangement shown in Figure 5.4a. As the shaft is displaced axially the shaft rotates. The only consequence to this in our application is that we need to allow for it in sizing the cube corner reflectors if we wish to keep the beam all within one sector. This effect can also be reduced by making the diaphragm diameter larger. The other disadvantage is that as the shaft is displaced axially from its neutral position the radial stiffness decreases, making it more likely that the shaft could be displaced by external forces such as vibration. These weaknesses led to a search for an improved spring design. A sketch of the flexure spring design used for the SWIFTS breadboard is shown in Figure 5.4b. This design is credited to Ray Radebaugh at NIST. Although a detailed analysis was not performed on the design it is believed that it will allow a larger radial stiffness and less rotation for a given axial displacement than the simple diaphragm spring of figure 5.4a.

The displacement force was provided by a "voice coil" type driver built by BEI Motion Systems Company (BEI model no. LA26-29-000A). This is shown in Figure 5.3. The mirror shaft is attached to a coil wound on a thin shell. The stationary component is a SmCo permanent magnet built into the shape of a cup. When a direct current is applied to the coil it is attracted to the magnet, drawing it into the cup. One great advantage of this system is that if no ferrous metal components are used in the shaft construction near the magnet there will be no lateral forces on the shaft as the coil moves in and out of the magnet. The BEI actuator allows a total axial movement of the shaft of plus and minus 0.75 cm from its nominal center position, more than adequate for our design goal of 1 cm total. It has a force constant of 1.3 lb/amp and a winding resistance of 2.1 ohms. The thickness of material used in the flexure spring was adjusted to produce full deflection with the application of plus and minus 2 Amps, dissipating about 8 Watts in the coil. Since the radial stiffness of the flexure springs will be proportional to the axial stiffness, and, thus, to the required drive power, an analysis of the maximum expected radial forces in a flight instrument would allow the spring thickness to be adjusted for minimum power consumption. The BEI actuator is rated at about 80 Watts so it is capable of producing a much larger force than was user in the breadboard. In the SWIFTS breadboard the coil was attached to the mirror shaft and the heavy permanent magnet was attached to a stationary mount. This minimizes the radial load on the shaft. If there is a problem with dissipating the coil power in a flight instrument the coil and magnet could be reversed, allowing the coil to be attached to a fixed heat sink.

A few simple experiments were performed to evaluate the mirror suspension and drive system. The most significant one was to mount a flat mirror on the shaft in place of the cube corner reflector. This mirror was then observed with an autocollimator while current was applied to the drive coil to move the mirror axially. Within the sensitivity of the autocollimator, about 1 arc second, no angle change could be detected. Measurements of radial stiffness were not made but should be in order to fully evaluate the suspension system.

With the coil disconnected from the power source the shaft oscillates axially with a low damping factor, however, if the coil leads are shorted together the damping is very high. This suggests that the only launch lock mechanism needed is to short out the coil leads.

In a flight qualified design a detailed analysis of the effect of all expected forces must be made to determine the minimum required size for the mirror suspension and drive system. It is here that probably the greatest size reduction can be made.

#### 5.4 Reference laser

there are several problems with trying to use a HeNe gas laser in an instrument designed for use in space. High power consumption, large heat dissipation, and limited lifetime are a few of these. For this reason a solid state laser diode was chosen as the primary mirror position reference. A laser diode has high conversion efficiency from electrical input power to optical output power and if the junction is kept near room temperature the mean time to failure is on the order of  $10^5$  hours. There are, however, a few difficulties which need to be overcome, which we will discuss below. Figure 5.5 shows the optical path of the laser diode interferometer. It uses the same optical path through the instrument as the external light path except that it is positioned to use another sector of the cube corner reflectors. The diode output is collimated by a high quality lens into a bundle about 0.8 cm in diameter. After passing through the interferometer the light is collected by one of the lens/photodiode/preamplifier modules described in section 5.2. An optical arrangement was also tried (Figure 5.6) in which the laser reference beam was double passed through the moving mirror in order to get twice as many zero crossings for a given mirror distance. The scheme shown uses flat mirrors but in keeping with the design goal of no precision adjustments cube corner retroreflectors could be used. The only concern with retroreflectors is that they can feed back light into the laser, causing instability. This feedback can be eliminated by using an isolator consisting of a polarization rotator and polarizer to block the return light. After a brief test it was decided that the added complexity and additional space required of the doubling scheme did not give enough advantage to warrant its use, especially since it was desired to develop a position readout scheme which did not depend on zero crossings only (see section 4.5).

Figure 5.7 shows a scheme for providing direction sensing which can be used to keep track of absolute mirror position using zero crossings in both directions of mirror movement (see section 4.5). A wedged glass plate is added to one leg of the laser path to produce a small phase shift across the beam in one direction. A prism shaped mirror is then placed directly behind the focusing lens to divide the beam into two halves focused onto two separate detectors. Because of the difference in phase between the two halves of the beam, introduced by the wedged plate, the two output sinusoids will be slightly out of phase with each other. The output of two separate zero crossing detectors can then be used with a simple logic circuit and an up/down counter to keep track of absolute mirror position even when it reverses direction. This scheme was not actually implemented in the SWIFTS breadboard since our primary interest in the first stage of implementation was in single, non-reversing scans of data.

The laser diode used in the SWIFTS breadboard was a Hitachi HL7838G. This is a GaAlAs diode which operates at a wavelength of approximately 780 nm ( $12,820 \text{ cm}^{-1}$ ) and produces a maximum output power of 20 mW. The output was collimated by a Newport laser objective, model F-L20. Two properties of this diode need to be looked at in order

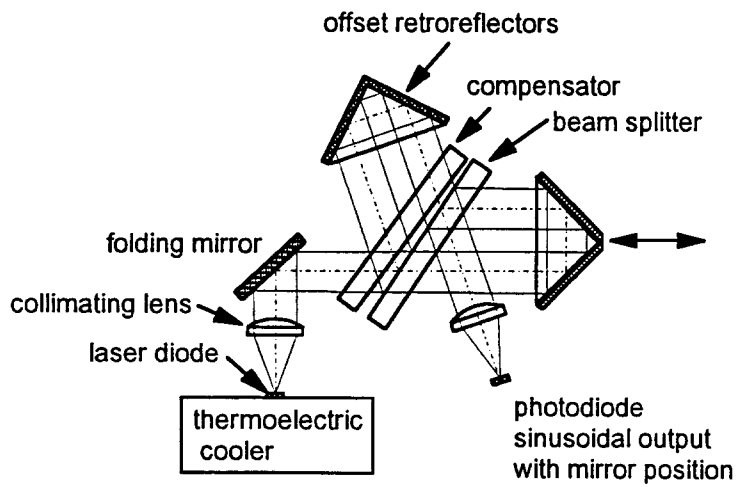


Figure 5.5 Optical Path of SWIFTS Laser Diode Interferometer

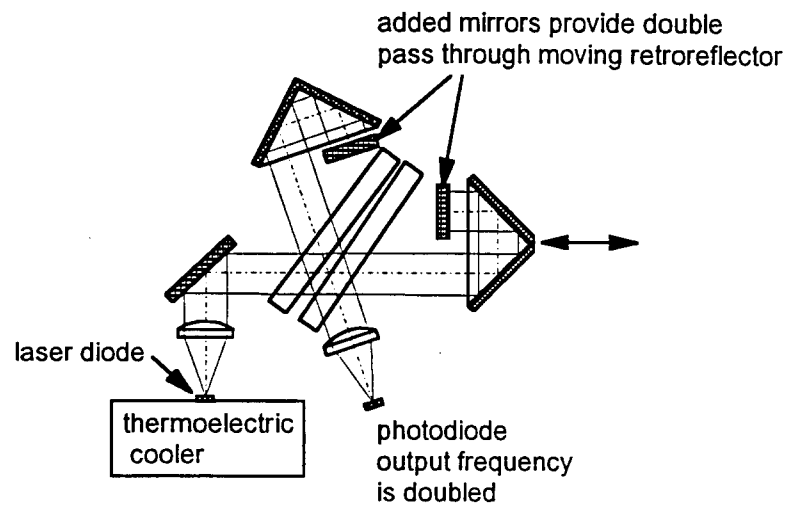


Figure 5.6 Reference Frequency Doubling Scheme

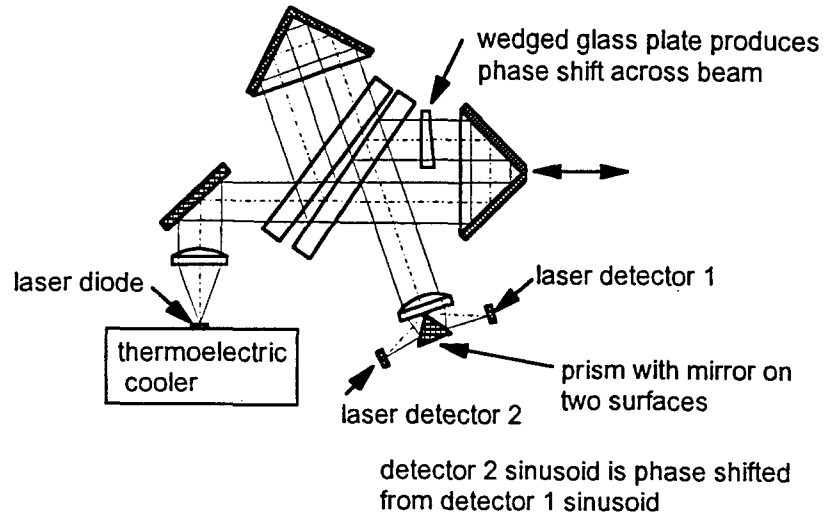


Figure 5.7 Laser Interferometer with Components Added for Direction Sensing

to use it as a reference in our application; one is coherence length and the other is wavelength stability. First we will look at coherence length. In our interferometer application we need a coherence length long enough to be able to move the mirror over its entire range of at least plus and minus 0.5 cm without seeing a significant reduction in amplitude of the sinusoidal output signal. Because of the very small cavity length (about 300 microns) of the laser diode the longitudinal modes are spaced much further apart in wavelength than those of a typical HeNe laser. According to the Hitachi data book this mode spacing is about 0.34 nm ( $5.6 \text{ cm}^{-1}$ ). What this means is that if the diode lases in more than one mode at a time the coherence length will be very short. The HL7838 was chosen because it was advertised to support only a single longitudinal mode. Other diodes in the same series lase simultaneously in several modes. This property was easy to test. After aligning the interferometer the mirror was moved over the desired range while observing the sinusoidal output on an oscilloscope. It was found that the coherence length could be varied by varying the amount of current applied to the diode. At low current, barely above the lasing threshold, the coherence length was very short; the mirror could be moved only about 1 mm for an amplitude reduction to about 10% of its peak value. At a current near the maximum rated value the amplitude only fell to about 90% of the peak when moved over the entire range of 1 cm. Thus, we conclude that, from the standpoint of coherence length, the HL7838 is suitable as long as it is operated at high current and as long as our position determining algorithm is able to handle the gradual falloff in amplitude of the sine wave with position.

The other concern is wavelength stability. Both long term and short term stability must be considered. Within its operating current and temperature range the laser wavelength can vary from 770 to 795 nm. Since this is the primary wavelength reference for the instrument any uncertainty in its value will lead to an equal uncertainty in the wavelength of the external light being measured. In some applications the scene may be self-calibrating; Fraunhofer lines or easily identifiable gas absorption lines in the scene can be used. Another possibility is to include a calibration source within the instrument, such as a low pressure gas lamp. The other more serious concern is short term stability. The diode output wavelength is dependent on both the case temperature and the current. If either of these fluctuates significantly during the measurement period it will produce the frequency modulation effect discussed in section 4.4. A gradual drift over the measurement time period would reduce the measurement resolution. For example, if the laser wave number changed by  $1 \text{ cm}^{-1}$  during the recording of an interferogram a spectral line at approximately the laser wavelength will be smeared out over a  $1 \text{ cm}^{-1}$  width. Since one of the SWIFTS breadboard design goals is to measure with a resolution of  $1 \text{ cm}^{-1}$  we will need to keep this short term stability down to much less than  $1 \text{ cm}^{-1}$ . Converting this to wavelength we desire a stability  $\ll 0.06 \text{ nm}$ .

Two things in the laser diode cause the emission wavelength to change, the band gap energy and the physical length of the cavity. Both of these result directly from temperature change. According to the Hitachi Optoelectronics Data Book the overall wavelength temperature coefficient is 0.25 nm/deg. C. A closer look shows that as the temperature is changed the diode makes abrupt wavelength changes in increments of 0.34 nm as it goes from one longitudinal mode to the next. If we confine our look to the region

between mode changes the temperature coefficient is only about 0.06 nm/deg. C. If we hold the case temperature of the diode constant and change the current there will be a temperature change of the junction due to the thermal resistance of the material. This results in a wavelength change with current of 0.006nm/mA (Crossdale and Palum 1990). We can now use this data to establish the necessary operating conditions required to meet our operating goal. It is immediately obvious that we must find a way to insure that we are not operating near one of the points at which a mode change is about to take place. We could find these points by using some means to observe the diode output wavelength while holding the current constant and gradually changing the case temperature. The operating temperature could then be chosen to be half way between two mode change temperatures. In an operational instrument it might be necessary to periodically check this operating point. We can then use the smaller temperature and current coefficients to establish requirements for stability. Let us choose a maximum allowable short term fluctuation of 0.006 nm, one tenth of the desired instrument resolution. We then calculate the required temperature stability to be plus or minus 0.05 deg. C. and the current stability to be plus or minus 0.5 mA. Although these are stringent requirements they are within the limits of available technology. For the SWIFTS breadboard the laser diode temperature was controlled by a thermoelectric cooler assembly manufactured by Newport Corp. It consists of an LDM100 TE cooled laser diode mount and a TC100 temperature controller. The diode current is controlled by a Newport PCS100 precision current source.

One final comment should be made about the reference laser diode. The diode used operates at 780 nm which is in the center of the wavelength range we desire to measure. Because of the high sensitivity of a FT spectrometer we might be concerned that even a small amount of light scattered into the signal channel from this laser could contaminate the spectrum being measured. This is of particular concern with a system like the SWIFTS breadboard which runs the laser path alongside the signal path. If this proves to be bothersome in practice we could completely separate the two paths, for example, by building a separate laser interferometer to operate off the back side of the moving mirror shaft. Whether or not this is necessary will have to be determined experimentally.

## **5.5 Electronics and signal processing**

The heart of the SWIFTS breadboard drive and signal processing system is an IBM compatible personal computer. An A/D converter board and a combined D/A converter and digital interface board were added to interface with an external box containing the spectrometer analog electronics and power supplies. In addition to a C programming language package two specialized commercial software packages were used, one for data acquisition and instrument control, and the other for processing the interferograms. No provision was made to collect data from all pixels of an imaging detector array since the principles could be demonstrated by looking at only one or two pixels at a time. A block diagram of the electronics system is shown in Figure 5.8.

The A/D converter is a National Instruments AT-A2150C. It has four analog input channels and uses a 64 times over sampling delta-sigma modulating converter with 16 bits of resolution. Its main features are true simultaneous sampling of all four channels, ultra

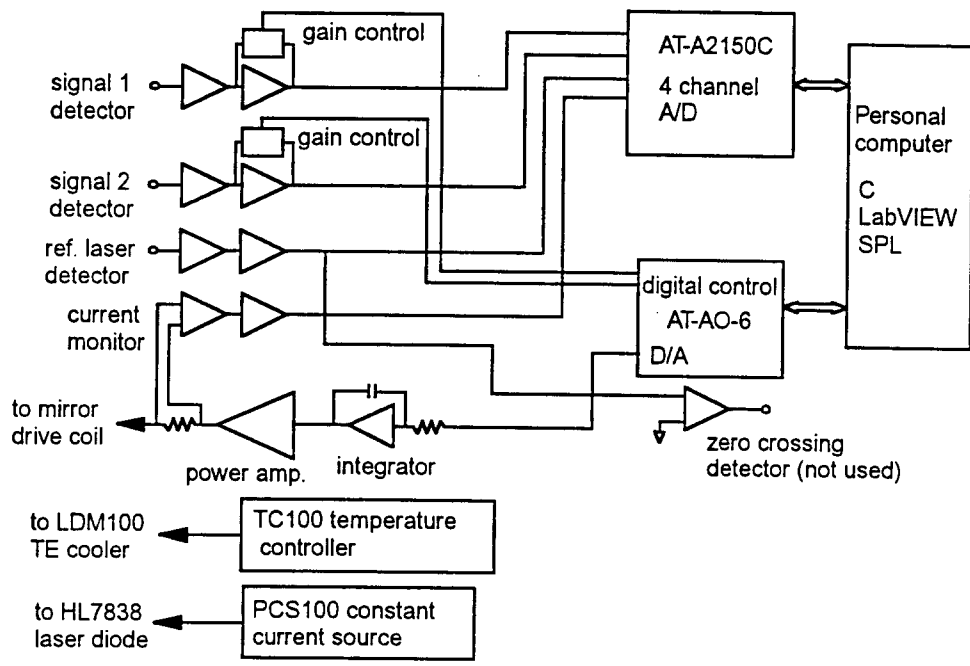


Figure 5.8 SWIFTS Breadboard Electronics Block Diagram

low distortion, built-in digital anti-aliasing filters, and a maximum sampling rate of 51.2 kHz. In the breadboard instrument all four inputs are used. Two inputs are for two signal channels, another is for the laser position reference, and the fourth is used to monitor the mirror drive coil current.

The two signal channels and one laser reference channel used 0.1 inch diameter silicon photodiodes (EG&G SGD-100) into transimpedance preamplifiers. It was also planned to use a large dynamic range imaging array being developed for another program but it was not available by the end of the SWIFTS program. Two stages of post amplification are provided for each channel before the A/D converter. The post amplifiers for the external signals have four bit digital gain control. Control is provided by the digital output of a National Instruments AT-AO-6 computer board. This gain control feature allows computer control of the amplifier gain to effectively increase the A/D resolution to 20 bits.

The output of the laser reference amplifier goes into one channel of the A/D converter for use by a computer algorithm which estimates the zero crossing times (see section 4.5 method 4). The amplifier output also goes to a comparator which generates a square wave transitioning at the zero crossings. Although not implemented in the first phase of testing, this output is available for tachometer control of the mirror drive and also to send an interrupt for the measurement of zero crossing times (section 4.5 method 3).

Mirror drive and control is accomplished by sending a voltage from the computer, provided by a D/A output of the AT-AO-6 computer board to an analog integrator. This integrator provides a ramp with a slope dependent on the input voltage supplied. The output of the integrator then goes into a power amplifier which is connected to the mirror drive coil. Because of non-linearity in the mirror drive a straight ramp will not provide constant velocity. In order to provide a constant velocity without using velocity feedback from the laser interferometer the drive current was monitored by the fourth channel of the A/D converter. Mechanical means was then used to determine mirror position as a function of drive current. A look up table in the computer then allows the current profile vs. time to be adjusted to provide near constant velocity. Providing the computer control through a ramp generator was chosen in order to minimize the time spent by the computer in velocity control. The ramp only needs to be adjusted a few times during the mirror travel to provide nearly constant velocity. In retrospect we believe mirror velocity control could have been provided more simply as a function external to the computer with the computer providing only the start and stop signals and a single digital word containing the desired velocity. Velocity feedback from the laser interferometer would then take the place of the lookup table and also provide a much more precise control. This was not done originally because it was desired to provide a means of mirror movement independent of the optical configuration.

Software control of the AT-A2150C and AT-AO-6 boards is provided by LabVIEW for Windows, also a National Instruments product. For the first phase of testing, software control allowed the mirror to be positioned at either end of travel, run at a controlled velocity, and a specified number of data samples to be taken and stored after a specified time delay from start of scan. SPL--Spectral Processing Language for FTIR

Spectroscopy, by ONTAR Corporation, was also purchased to perform standard processing, analysis and display of the interferogram data. Two main tasks of SPL are to perform phase correction of the interferogram and to perform the FFT to recover the spectrum from the interferogram.

## 6.0 Results and conclusions

By the end of the time allocated for this program all equipment was assembled, aligned, and tested but no interferograms were processed. Nevertheless, most of the other goals were achieved. Some of the more significant findings from this study are listed below:

1. One of the first concerns of an instrument designer should be to select the best method for making a given measurement. In the case of spectral measurements at a resolution of  $1 \text{ cm}^{-1}$  both the FT interferometer and the diffraction grating instrument must be considered. In section 3 some criteria were established for making this decision. It was determined that even with reasonable field-of-view restrictions imposed by a detector array the FT instrument offers a much greater throughput than the grating instrument for a given collection aperture diameter. What this means in a practical sense is that for a given measurement accuracy the FT instrument should be able to perform the measurement in much less time. For a space-borne instrument this might mean that many more scenes could be examined in a single pass of the satellite. However, we must also consider the ability of a computer system to keep up with this faster data flow.

It was also found that source intensity fluctuations can be more detrimental to the FT instrument. In section 4.2 two methods were discussed for reducing the effects of fluctuations originating at the source or in the atmosphere. One uses a ratio technique in which the interferogram is divided by the total signal intensity. In the other, two signals are generated 180 degrees out of phase and subtracted. Although both of these methods can be effective in the right situations it was shown that neither was capable of eliminating all effects of signal fluctuation and that what remains could have a worse effect on the accuracy of measurement than it does on the grating instrument.

In section 3.3 we also found that quantization noise can seriously limit the achievable accuracy of the interferometer, requiring many more bits of A/D converter resolution to achieve a given measurement accuracy than does the grating instrument. This could be a serious limitation, especially for a system using a detector array of limited dynamic range.

Putting all this together we could conclude that if time available for the measurement is a primary concern then the FT interferometer offers the best possibility for reducing that time. If source fluctuation or quantization of the dynamic range are the limiting factors then a grating instrument should be seriously considered.

A final criterion for instrument type selection was discussed in section 3.2. For an imaging spectrometer requiring a large number of spectral and spatial elements, the interferometer may offer the simplest instrument design to implement.

2. In section 4 requirements were established for the sample interval generator. In a short wavelength instrument, or in an instrument using a sequentially read out detector array, the traditional technique of using zero crossings of a laser interferometer were shown to be inadequate. Two methods were discussed which use a digital filter algorithm to determine the mirror position at any point in time and which do not require precise velocity control of the moving mirror. A computer simulation of one of these techniques has demonstrated that it appear to be very adequate.

3. A versatile breadboard was built which allows testing of a number of data sampling methods and source fluctuation cancellation methods. In accordance with the original goals this design requires no precision alignment of the separate components. The mirror suspension and drive system were demonstrated to be more than adequate for our purposes and have no parts requiring lubrication. We can assume that the lifetime of the suspension system would be virtually unlimited in a space application. The problem of a reliable position reference was solved using a temperature and current stabilized laser diode. Its wavelength stability was determined to be adequate by calculation and its coherence length was demonstrated to be adequate over the entire range of mirror travel.

From this study we can conclude that, from the standpoint of the optical, mechanical, and sampling interval generation, there appear to be no insurmountable obstacles to building a space qualified instrument with the desired accuracy and wavelength region. However, during the study several problem areas have been identified which we believe would be worth further study. The first of these has to do with on-board data processing and storage. As shown by simple example in section 4.6.5 an imaging FT spectrometer is capable of generating a very large amount of data in a short period of time. After the data is corrected for position and phase dispersion, and transformed into its spectrum, it is likely that, for any given experiment, only a relatively small amount of data will be kept. For example we may be interested in only the relative intensity of twenty spectral components out of 20,000. A study should be done to determine how to reduce the required amount of intermediate data storage.

Another area of further study that could prove very fruitful is to look at alternative optical configurations. Although the scheme presented in this study appears to be adequate, it is quite large. A method which requires less precision in the sampling interval generating scheme would also be very desirable. For example, changing the optical thickness of a piece of glass in one of the interferometer legs can be done in such a way that a large movement of the glass produces a relatively small change in path length. This suggests that the required measurement interval could be determined by some means less accurate, and simpler, than the laser interferometer. Eliminating the laser path might allow the retroreflectors to be used without offset, affording a much more compact arrangement.

## References

- J. Brault, 1996, New approach to high-precision Fourier transform spectrometer design, *Applied Optics*, vol. 35, no.16, pp. 2891-2896.
- F. Crosdale, and R. Palum, 1990, Wavelength control of a diode laser for Distance Measuring Interferometry; *Laser-Diode Technology and Applications II*, SPIE vol. 1219, pp. 490-501.
- T. Hirschfeld, 1979, Digitization Noise in Fourier Transform Infrared Spectroscopy and Gain Ranging; *Applied Spectroscopy*, vol. 33, no. 5, pp. 525 - 527.
- L. Mertz, 1965, *Transformations in Optics*, John Wiley & Sons, Inc.- New York.
- E. Wolf, 1967, *Progress in Optics*, vol. IV, North-Holland Publishing Company - Amsterdam



DISTRIBUTION;

- 1 Russ Abbink  
101 Rainbow Dr. #N607  
Livingstone, Tx 77351-9300
- 1 MS 0972 Andy Boye, 5705
- 1 MS 0967 Steven Gentry, 5725
- 1 MS 0967 Carter Grotbeck, 5725
- 1 MS 0967 Tammy Henson, 5725
- 1 MS 1423 Gerald Hays, 1128
- 1 MS 0972 Anthony Medina, 5722
- 1 MS 0967 Brian Stallard, 5725
- 1 MS 0603 Bill Sweatt, 5725
- 1 MS 0603 Mial Warren, 1312
- 1 MS 9018 Central Technical Files, 8940-2
- 5 MS 0899 Technical Library, 4414
- 2 MS 0619 Review & Approval Desk, 12690  
For DOE/OSTI



DISTRIBUTION;

- 1 Russ Abbink  
101 Rainbow Dr. #N607  
Livingstone, Tx 77351-9300
  
- 1 MS 0972 Andy Boye, 5705
- 1 MS 0967 Steven Gentry, 5725
- 1 MS 0967 Carter Grotbeck, 5725
- 1 MS 0967 Tammy Henson, 5725
- 1 MS 1423 Gerald Hays, 1128
- 1 MS 0972 Anthony Medina, 5722
- 1 MS 0967 Brian Stallard, 5725
- 1 MS 0603 Bill Sweatt, 5725
- 1 MS 0603 Mial Warren, 1312
- 1 MS 9018 Central Technical Files, 8940-2
- 5 MS 0899 Technical Library, 4916
- 2 MS 0619 Review & Approval Desk, 12690  
For DOE/OSTI

